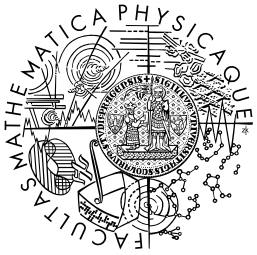

FACULTY
OF MATHEMATICS
AND PHYSICS
Charles University

BACHELOR THESIS

Dominika Hubová

Mass Loss from Binary Stars

Institute of Theoretical Physics

Supervisor of the bachelor thesis: Mgr. Ondřej Pejcha, Ph.D.

Study programme: Physics

Study branch: General Physics

Prague 2018

I declare that I carried out this bachelor thesis independently, and only with the cited sources, literature and other professional sources.

I understand that my work relates to the rights and obligations under the Act No. 121/2000 Sb., the Copyright Act, as amended, in particular the fact that the Charles University has the right to conclude a license agreement on the use of this work as a school work pursuant to Section 60 subsection 1 of the Copyright Act.

In Prague 17.7.2018

I would like to express my deepest gratitude to my supervisor Mgr. Ondřej Pejcha, Ph.D for his generous help, valuable advice and his patient guidance not only throughout writing this thesis.

I am also very grateful to my whole family for their support and understanding and to my friends, who always helped me up and forwards when I lost my footing.

Finally, my gratitude belongs to my Mountain, who gave me courage to start, strength to finish and everything he could in between.

Title: Mass Loss from Binary Stars

Author: Dominika Hubová

Institute: Institute of Theoretical Physics

Supervisor: Mgr. Ondřej Pejcha, Ph.D., Institute of Theoretical Physics

Abstract: In this thesis we investigate the loss of mass from binary systems from the vicinity of the second Lagrange point L2. This phenomenon arises mainly in the common envelope evolutionary phase of close binary systems when the cores of the components orbit inside a shared gaseous envelope. It is a crucial but poorly understood stage in the system's development with two substantially different possible outcomes – stellar merger or formation of a close binary system with compact components. Modifying mass, energy and angular momentum of the binary, mass loss through the L2 point might significantly impact the system's evolution throughout the common envelope phase. Using numerical integration of equations of motion, we evaluate final states of test particles ejected from the proximity of the L2 point with arbitrary initial velocity with respect to the corotating reference frame. Furthermore, we compute the amount of energy and angular momentum these particles carry away from the system. Previously, only the particles ejected from the L2 point from initial corotation were studied; this work is therefore the first to address this problem with general initial conditions. Firstly, we initiate the particles at the L2 point with velocity pointing in the direction of x-axis and y-axis. Secondly, we eject the particles from corotation from the area surrounding the L2 point. Finally, we study the behaviour of particles that are ejected from the neighbourhood of the L2 point with radial velocity and with tangential velocity pointing in and opposite to the direction of system's rotation. In most cases we found a set of initial conditions allowing the particle to escape from the system to infinity.

Keywords: binary systems; mass loss; second Lagrange point; numerical integration;

CONTENTS

CHAPTER 1

INTRODUCTION: STELLAR MASS LOSS AND ITS CONSEQUENCES

The subject of stellar evolution plays an important role in our understanding of the Universe – from the question of behaviour and fate of our Sun (and consequently of the entire Solar System), through the reasoning behind various observable phenomena such as novae and supernovae, to the problem of general constitution of the Universe and origin of more exotic objects like neutron stars and black holes. Different stages of a star's life and numerous processes that accompany its evolution strongly depend on individual characteristics such as mass, chemical composition, rotation and the star's surroundings (e.g. binarity). For example, more massive stars have generally shorter lifetimes that lead to the formation of neutron stars or black holes during a supernova explosion, whereas stars with low to intermediate mass live longer and end their evolution as white dwarfs (Langer 2012).

However, even the mass of a star can dynamically and irregularly change during the star's existence, altering the subsequent evolutionary path. Almost omnipresent and incessant phenomenon generating mass loss in single stars is steady stellar wind (Lamers & Cassinelli 1999), whose effects are most pronounced in the evolution of massive stars. According to Smith (2014), throughout their lifetime, massive stars can shed by wind a significant fraction of their initial mass. Consequently, the rate of mass loss influences the type of eventual supernova explosion and its remnant (Heger et al. 2003). Moreover, some single stars can lose portions of their mass abruptly by eruptions and explosions, as is observed for example during the flare-ups produced by stars known as luminous blue variables (Humphreys & Davidson 1994).

Furthermore, a considerable amount of observable stars was detected to have a binary companion (Sana et al. 2012). In binary systems, which are therefore just as significant as single stars, even more processes leading to changes in stellar masses can arise. These are most pronounced in close binary systems, where the distance between the components is sufficiently small and the shape of the stars is distorted by their mutual gravitational influence. If one of the components (called the donor) of such system fills its Roche lobe — the boundary enclosing the area where matter remains gravitationally bound to said component — mass will flow onto its companion (the accretor) in a process called the Roche lobe overflow (RLOF). The mass is transferred from one star to the other through the inner Lagrange point L1, which is one of the five locations in the surroundings of the

binary system where the gravitational influence of the components compensates the centrifugal force of the system's rotation.

The onset of RLOF can be caused by the expansion of the donor due to its individual stellar evolution. Alternatively, loss of angular momentum (for example by magnetic braking or gravitational radiation from the binary system) may also lead to RLOF, because it is usually accompanied by the decrease in the orbital separation between the components and consequent shrinking of the Roche lobes. Once initiated, the characteristics of mass transfer depend mainly on the properties of individual components (e.g. the evolutionary stage and structure of the donor, the type of the star undergoing mass gain) and on their mass ratio. The process is self-influencing – mass transfer changes the mass ratio of the binary, which modifies sizes and shapes of the Roche lobes, which can then power further mass transfer or, to the contrary, interrupt the process entirely. Orbital period and separation between the components may vary too. Predicting the outcome of the RLOF and further evolution of the system thus becomes much more complicated compared to the development of a binary with distant components which do not have a substantial influence on each other. Furthermore, mass transfer uncovers new evolutionary paths, and it can produce various observable phenomena or objects that would be otherwise impossible.

Based on the difference between the amounts of mass lost from the donor and gained by the accretor we distinguish two types of RLOF. If all of the matter leaving the donor star gets captured by its companion and hence no amount of mass and angular momentum is lost from the system, we talk about conservative mass transfer. However, a substantial portion of matter can be entirely lost from the binary into its surroundings during the accretion by the mass gainer (one such scenario was presented by Van Rensbergen et al. 2008). These systems are said to undergo non-conservative mass transfer. To this day, numerous models of binary evolution that take into account possible mass and angular momentum loss from the system during the mass transferring phase have been proposed (e.g. De Loore & De Greve 1992, Sepinsky et al. 2009). For instance, non-conservative RLOF was used by Giuricin & Mardirossian (1981) or Van Rensbergen et al. (2010) for modelling the observations of certain Algol variables, which are a class of eclipsing binary systems where the less massive component fills its Roche lobe.

More information on the mass transfer and possible mass loss by the Roche lobe overflow may be found for example in Harmanec & Brož (2011), Eggleton (2006) and Ivanova (2015).

1.1 Mass loss from the second Lagrange point

Another possible mechanism of mass loss from close binary systems appears in the contact stage of their evolution when the common binary surface comes into contact with the outer Lagrange point L2. As was first noted by Kuiper (1941), in such situations, matter — and thus energy and angular momentum — can be ejected from the binary from the vicinity of the L2 point, forming a spiral-shaped stream around the system.

1.1.1 Significance of the L2 mass loss

Mass loss from the L2 point is usually associated with the common envelope phase in the evolution of close contact binaries. This is a brief stage during the system's lifetime when the cores of the components orbit each other inside a shared gaseous envelope, occurring when one of the components gets engulfed in its companion's atmosphere, either as a result of expansion or decrease of orbital separation (Paczynski 1976, Ivanova et al. 2013). Even though quite short-lived, the common envelope evolutionary phase plays a crucial role in the binary's development. Nevertheless, our understanding of all of its accompanying phenomena and the implications they have on the system is to this day still quite insufficient.

Currently, it is widely accepted that the common envelope gives rise to processes responsible for a rapid decrease in the distance between the binary components. Due to this orbital tightening, the common envelope phase may be a sign of ensuing coalescence of the binary components which may lead to new objects with possibly interesting properties. However, this outcome is not necessary, as the envelope might get ejected from the system, hindering the merger and leaving the remnants orbiting each other at a relatively small distance.

The latter scenario was proposed as an explanation of the origin of various very close binary systems where the observed orbital separation between the components is orders of magnitude smaller than would have been possible for their progenitors. Thus undergoing common envelope evolution is thought to be inevitable for the formation of cataclysmic variables, composed of a white dwarf and a main-sequence star, or X-ray binaries, which consist of a neutron star or a black hole and an ordinary star (Iben & Livio 1993, Tauris & Van Den Heuvel 2006). Furthermore, recent launch of LIGO and Virgo interferometers and ensuing several successful detections of gravitational waves (Abbott et al. 2016*a*,*b*, 2017*a*,*b*) have called attention to the question of development of binary black hole or neutron star systems responsible for these signals. One proposed channel, discussed for example by Tauris & Van Den Heuvel (2006) and Belczynski et al. (2016), is through the classical evolution of isolated binary star systems. To obtain the relatively small distance between the compact objects which is required for them to merge by gravitational radiation within the Hubble time, the authors suggest that these systems must evolve through at least one common envelope phase without the components coalescing prematurely. But as such evolution is not well understood and the conditions for timely envelope ejection are unclear, models of this evolutionary path are rather uncertain.

As the surface of the binary in the common envelope evolutionary phase usually exceeds the L2 point, matter can be ejected from the system. The resulting loss of mass and angular momentum may have some influence over the development of the binary and the outcome of the common envelope phase, as it may be one of the processes affecting whether the components would merge before the envelope is ejected.

Moreover, Linial & Sari (2017) have suggested that L2 mass loss may also occur under specific conditions when the distance between the components decreases gradually due to some unspecified external process (such as gravitational radiation, dynamical friction, tidal evolution or magnetic braking), but no common envelope is formed. They show that if the orbital evolution is fast enough

and the mass ratio of the binary is extremely small, the less massive component may not only exceed its Roche lobe and initiate mass transfer by RLOF, but also eject matter through the L2 point. This is possible because in systems with small mass ratios, the distance between the L1 and L2 equipotential surfaces is quite small, comparable with the depth from which material is released through the L1 point. Considering the emission of gravitational radiation as the mechanism responsible for the shortening of orbital separation, the authors argue that L2 mass loss might influence the gravitational wave signal produced by mergers of super-massive black holes and main-sequence stars, which could be observed by future gravitational wave detectors.

1.1.2 Kinematics of the L2 mass loss

The idea that binary systems may lose matter by the outer Lagrange point was first formulated by Kuiper (1941) while he was trying to explain photometric and spectral properties of the variable star β Lyrae. In his work, Kuiper (1941) calculated and visualised several orbits of test particles in the proximity of the binary by direct numerical integration of their equations of motion, noting that some of them are able to leave the system through the neighbourhood of the L2 point and fly away. Even though his model of β Lyrae based on observational phenomena produced by the mass loss stream was later rejected, the proposed concept of mass loss from the L2 point was studied more profoundly.

At first, Webbink (1976) and Nariai & Sugimoto (1976) noted that due to the mass and angular momentum loss from the L2 point, the distance between the components in the common envelope phase decreases, which then drives further mass loss and further orbital tightening in the system. Analogous reasoning was used for example by Flannery & Ulrich (1977) to explain the origin of some cataclysmic variable stars, or by Livio et al. (1979) while modelling the development of planetary nebulae with a close binary system in its centre. However, Meyer & Meyer-Hofmeister (1979) pointed out that assumptions of these models, which require that the envelope rotates at the same rate as the components all the way to the L2 point, are rarely satisfied in real systems. As the envelope during the inspiral of the components revolves much slower than the components themselves, and the pressure on the surface of the envelope is usually relatively small, the matter around the second Lagrange point does not have sufficient velocity to leave the system. Therefore, no significant mass loss that would influence the binary should appear. Meyer & Meyer-Hofmeister (1979) argued that even though the decrease in orbital separation does occur in the common envelope phase, its main cause is the frictional drag issued between the cores and the envelope.

Around the same time, Shu et al. (1979) tried to establish dynamical properties of the mass loss stream leaving from the second Lagrange point. They investigated for which values of mass ratio will the matter become unbound and escape from the system to infinity or whether it will otherwise form an excretion disc around the binary. Additionally, they computed the amount of energy and angular momentum carried away from the system by test particles ejected from the L2 point, also as a function of the system's mass ratio. Their results show that in systems where mass ratio $q \in (0.064, 0.78)$, particles escape from the binary to infinity with positive final energy. On the other hand, the matter

stays bound to systems whose mass ratio is either too small ($q < 0.064$) or too big ($q > 0.78$), the energy of the particles in their final state being negative. In the first case, the authors argue that the less massive component is not massive enough to exert the torque the matter would need to become unbound from the system. In the second case, the matter at the L2 point is too strongly bound to the system because the masses of the components are comparable, and again the torque exerted by the less massive star is not enough to throw the matter to infinity.

However, throughout all of the calculations performed by Shu et al. (1979), the particles leaving the system from the second Lagrange point were initially in corotation with the binary. During the presentation of their results, Shu et al. (1979, p.234) alert the reader to the fact that "*the small surface pressure forces at the top of the common envelope of a contact binary may never be able to overcome the combined inertial and gravitational forces if the matter rotates sufficiently slower than synchronously that the latter combination is always confining. It remains to be seen, therefore, how special a case is represented by [our] solution for the mass loss problem from the L2 region.*" Considering these restrictions on its occurrence, the interest in L2 mass loss began to decline and more studies were not carried out.

Nonetheless, mass loss from the L2 point might occur during early stages of binary mergers. This possibility was lately reinforced by numerous numerical hydrodynamical simulations of binary coalescence, which displayed a stream of matter spiraling around the binary, as can be seen for example in the works of Lombardi Jr et al. (2011), Ivanova et al. (2013), Nandez et al. (2014) or MacLeod et al. (2018). In this context, it is likely that most of the matter ejected from the system was not initially in corotation with the binary components.

The first observed coalescence of a binary system was recognised in the eruption V1309 Scorpii, a member of a class of transient events know as luminous red novae, which was observed in September 2008 (Tylenda et al. 2011). Later, it was proposed by Pejcha (2014) that the merging binary might have experienced loss of mass and angular momentum from the L2 point, which would explain the light curve and the decrease in orbital separation. This claim was also supported by Zhu et al. (2016) or Tylenda & Kamiński (2016). Afterwards, dynamical and radiative properties of the matter stream ejected from a binary system during a merger have been simulated (Pejcha et al. 2016*a*,*b*) and applied to V1309 Scorpii to show that mass loss played a crucial role in its evolution (Pejcha et al. 2017). However, in all of the models, the ejected matter was presumed to be initially in corotation with the binary system, an assumption that may be strongly violated in late stages of the simulations.

1.2 Goals and overview of this thesis

The main goal of this thesis is to determine final states of particles ejected from a binary system from the proximity of the L2 point with general initial velocity. We use numerical integration of equations of motion to establish trajectories of these particles and to compute the amount of energy and angular momentum they carry away from the system. This is the first step to better understand the influence of the L2 mass loss on binary systems and to improve proposed models

of binary evolution.

In Chapter 2, we introduce a simple way to express the gravitational influence of a binary system that arises due to the transformation into a non-inertial frame of reference which corotates with the binary components. Moreover, we derive the equations describing the motion of test particles in this frame and also the relations between the particle's position and velocity with respect to the corotating system and its energy and angular momentum that would be measured by an inertial observer.

Chapter 3 describes the setting of the problem and the numerical approach we used to compute the values of energy and angular momentum of test particles in their final states. We specify possible outcomes of the integration and how we treated those situations.

Finally, Chapter 4 contains a summary of our results and their discussion. At first, in section 4.1, we compare our results with those calculated by Shu et al. (1979). In section 4.2 we abandon the assumption of initial corotation at the L2 point and eject the particles with velocity pointing in a specific direction. Section 4.3 contains results for particles ejected from the surroundings of the L2 point from corotation with the system. Finally in sections 4.4 and 4.5 we relax both assumptions of initial corotation and initial position at the L2 point and we study particles ejected from the neighbourhood of the L2 point with the velocity pointing in radial and tangential direction, respectively.

CHAPTER 2

BINARY SYSTEMS AND THEIR GRAVITATIONAL INFLUENCE

In this thesis we investigate the motion of particles in a binary system. We assume that the mass of the particles is negligible with respect to the masses of the binary components. The task is thus approached as a restricted three-body problem in which the test particles do not affect the gravitational field around the binary.

2.1 The Roche potential

To describe the gravitational field formed by a binary system, we will idealize its components as two point masses M_1 and M_2 revolving around their common centre of mass on circular orbits. Without loss of generality, we will assume that $M_2 \leq M_1$. Let a denote the separation between the centres of the stars (semi-major axis of the binary), T the orbital period of the system and $\boldsymbol{\omega}$ its orbital angular velocity. Applying Kepler's laws, these values are connected by relation

$$\omega^2 = \frac{GM}{a^3} = \left(\frac{2\pi}{T}\right)^2, \tag{2.1}$$

where $M = M_1 + M_2$ is the total mass of the binary system and G represents the universal gravitational constant.

The gravitational influence of a binary system is most easily expressed in the non-inertial Cartesian reference frame whose origin is placed at the centre of mass of the system and which rotates with the same angular velocity $\boldsymbol{\omega}$ as the binary. In such *corotating system*, the positions of individual components of the binary do not change in time, which leads to a significant simplification. Relative to this frame, the acceleration of a particle positioned at $\mathbf{r}$ moving with the velocity $\dot{\mathbf{r}}$ will be given by

$$\ddot{\mathbf{r}} = -\nabla\phi_R(\mathbf{r}) - 2\boldsymbol{\omega} \times \dot{\mathbf{r}}, \tag{2.2}$$

where

$$\phi_R(\mathbf{r}) = -\frac{GM_1}{|\mathbf{r} - \mathbf{r_1}|} - \frac{GM_2}{|\mathbf{r} - \mathbf{r_2}|} + \frac{1}{2}|\boldsymbol{\omega} \times \mathbf{r}|^2 \tag{2.3}$$

is known as the *Roche potential*. Vectors $\mathbf{r_1}$ and $\mathbf{r_2}$ represent the positions of the centres of the stars in the corotating frame of reference. The third term in

equation (2.3) leads to the centrifugal acceleration, whereas the second term in equation (2.2) represents the Coriolis acceleration[1].

In this thesis, we set the corotating system in a manner that the stars are positioned on the x-axis, with the less massive star on the positive side, and that the axis of rotation is identical with the z-axis ($\boldsymbol{\omega}/\omega = \mathbf{e}_z$). Moreover, we adopt a as the unit of length and $a\omega$ as the unit of velocity. Denoting the *mass ratio* of the stars by

$$q = \frac{M_2}{M_1} \in (0, 1] \tag{2.4}$$

and introducing the parameter

$$\mu = \frac{M_2}{M_1 + M_2} = \frac{q}{1+q} \in (0, 1/2]\,, \tag{2.5}$$

it is possible to rewrite the Roche potential as[2](Shu et al. 1979)

$$\phi_R\,(x, y, z) = -\frac{\mu}{\sqrt{(x-1+\mu)^2 + y^2 + z^2}} - \frac{1-\mu}{\sqrt{(x+\mu)^2 + y^2 + z^2}} - \frac{1}{2}\left(x^2 + y^2\right), \tag{2.6}$$

depending only on the parameter μ, and thus only on the mass ration q of the binary components. Throughout this thesis, we will always consider the expression (2.6) when referencing to the Roche potential.

2.1.1 The Lagrange points

Characteristic for the Roche potential are five stationary points, called the *Lagrange points* or the *libration points*, whose position can be determined from the equation $\nabla\phi_R = 0$ (Harmanec & Brož 2011). Relation (2.3) implies that at the Lagrange points, the centrifugal force of the corotation and the gravitational force of the binary are in balance, consequently rendering a light object orbiting in any of them and affected only by gravity motionless relative to the binary system.

Lagrange points are situated in the plane of rotation of the binary. Three of them lie on the line connecting the two bodies – one in between, usually denoted by L1, and one on either side of the binary, where the typical notation is L2 for the point on the side of the less massive star and L3 for the one closer to the more massive component. The remaining two points, L4 and L5, form equilateral triangles with the stars (see Figure 2.1).

Specifically, the x-coordinate of the first three Lagrange points in the corotating system introduced above x_{Li} satisfies the equation

$$x_{Li} - \frac{\mu\,\mathrm{sgn}(x_{Li} - 1 + \mu)}{(x_{Li} - 1 + \mu)^2} - \frac{(1-\mu)\,\mathrm{sgn}(x_{Li} + \mu)}{(x_{Li} + \mu)^2} = 0 \tag{2.7}$$

with the conditions $x_{L3} < -\mu$, $x_{L1} \in (-\mu, 1-\mu)$ and $x_{L2} > 1-\mu$.

As can be seen in Figure 2.1, the first three Lagrange points are saddle points, while L4 and L5 points are local maxima of the Roche potential. Moreover, L1,

[1] As we assume constant orbital angular velocity of the binary system and thus uniform rotation of the corotating frame of reference, the Euler acceleration is zero.

[2] This expression evaluates the value of the Roche potential in the units of $a^2\omega^2$.

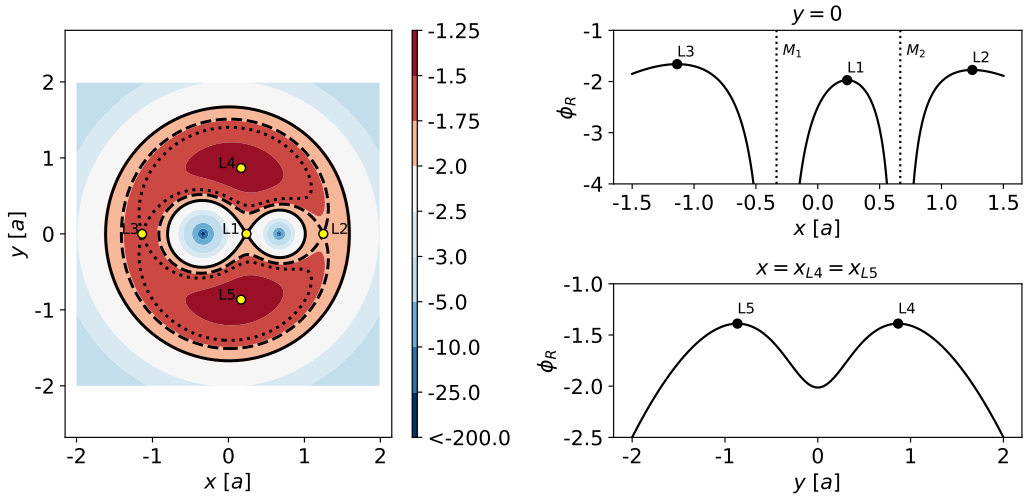

Figure 2.1: Visualisation of the Roche potential (2.6) in the plane $z = 0$ of the corotating frame of reference for a binary system with mass ratio $q = 0.5$. Picture on the left displays equipotential surfaces and positions of the five Lagrange points, which are marked by yellow points. The two droplet-shaped outlines formed by the equipotential passing through the L1 point (solid curve in the form of the lemniscate) the Roche lobes. The dashed and dotted lines are equipotentials passing through the L2 and L3 points, respectively. Pictures on the right side show values of the Roche potential – the top picture along the x-axis, while the bottom one along the line connecting the fourth and fifth Lagrange points. Values of the Roche potential in the Lagrange points are marked by the black points. The dotted vertical lines in the top right panel mark the locations of the binary components.

L2 and L3 points are dynamically unstable, and for the most values of mass ratios q, so are the points L4 and L5. The only exceptions are in systems with relatively small mass ratios ($q < 0.04$ approximately), where L4 and L5 represent stable equilibria (Danby 1992).

2.1.2 Classification of binary systems

Considering the Roche model of the gravitational field generated by a binary system, the most significant equipotential line is the line passing through the first Lagrange point L1. Resembling the lemniscate, this line encloses the areas where matter stays gravitationally bound to the component in its centre. These boundaries are called the *Roche lobes*, and they play a vital role during the system's evolution (see Chapter 1).

If the distance between the components is comparable with their diameters, the binary system is said to be *close*. As a star in hydrostatic equilibrium must fill a closed equipotential surface of the Roche potential, in these close systems, the stars' shapes are distorted by the common gravitational influence; their mostly spherically symmetrical bodies get deformed into pronounced droplet-like forms. According to the equipotentials that are filled by the components, we distinguish between three categories of close binary systems:

- *detached*, when both components occupy equipotentials smaller that their Roche lobes,
- *semi-detached*, when one component fills up its Roche lobe while the second remains smaller than the critical surface,
- *contact systems*, when both of the stars fill or even overfill their Roche lobes.

As was mentioned in Chapter 1, semi-detached and contact binary systems undergo mass transfer through the L1 point during the Roche lobe overflow, which may be conservative or non-conservative. Furthermore, when the common surface of a contact binary exceeds the L2 point, the system might also lose matter completely by a stream forming a spiral around the binary. This thesis focuses on trajectories of individual test particles leaving such systems from the proximity of the L2 point with arbitrary initial velocity.

2.2 Equations of motion and the Jacobi constant

Combining relations (2.2) and (2.6), the motion of a point particle in the corotating frame of reference can be described by the following system of three ordinary differential equations of second order:

$$\begin{aligned}\ddot{x} &= -\frac{\partial \phi_r}{\partial x}(x,y,z) + 2\dot{y} = \\ &= x - \frac{\mu\,(x-1+\mu)}{\left[(x-1+\mu)^2+y^2+z^2\right]^{3/2}} - \frac{(1-\mu)\,(x+\mu)}{\left[(x+\mu)^2+y^2+z^2\right]^{3/2}} + 2\dot{y}, \quad (2.8a)\end{aligned}$$

$$\begin{aligned}\ddot{y} &= -\frac{\partial \phi_r}{\partial y}(x,y,z) - 2\dot{x} = \\ &= y - \frac{\mu\; y}{\left[(x-1+\mu)^2+y^2+z^2\right]^{3/2}} - \frac{(1-\mu)\, y}{\left[(x+\mu)^2+y^2+z^2\right]^{3/2}} - 2\dot{x}, \quad (2.8b)\end{aligned}$$

$$\begin{aligned}\ddot{z} &= -\frac{\partial \phi_r}{\partial z}(x,y,z) = \\ &= -\frac{\mu\; z}{\left[(x-1+\mu)^2+y^2+z^2\right]^{3/2}} - \frac{(1-\mu)\, z}{\left[(x+\mu)^2+y^2+z^2\right]^{3/2}}. \quad (2.8c)\end{aligned}$$

To find their solutions, and thus to obtain the trajectory of the particle in the corotating system, a set of six initial conditions is needed – three specifying the initial position of the particle (x_0, y_0, z_0) and three defining the value and the direction of initial velocity $(\dot{x}_0, \dot{y}_0, \dot{z}_0)$.

An integral of motion can be found by manipulation of the equations of motion. Multiplying the relations (2.8a), (2.8b) and (2.8c) by $2\dot{x}$, $2\dot{y}$ and $2\dot{z}$ respectively and adding up the obtained equalities, we receive

$$2\dot{x}\ddot{x} + 2\dot{y}\ddot{y} + 2\dot{z}\ddot{z} = -2\frac{\partial \phi_R}{\partial x}\dot{x} - 2\frac{\partial \phi_R}{\partial y}\dot{y} - 2\frac{\partial \phi_R}{\partial z}\dot{z}. \quad (2.9)$$

Noticing that

$$2\dot{x}\ddot{x} = \frac{\mathrm{d}}{\mathrm{d}t}\dot{x}^2 \tag{2.10}$$

and

$$\frac{\partial \phi_R}{\partial x}\dot{x} + \frac{\partial \phi_R}{\partial y}\dot{y} + \frac{\partial \phi_R}{\partial z}\dot{z} = \frac{\mathrm{d}\phi_R}{\mathrm{d}t}, \tag{2.11}$$

equation (2.9) can be rewritten into

$$\frac{\mathrm{d}}{\mathrm{d}t}\left(\dot{x}^2 + \dot{y}^2 + \dot{z}^2\right) = -2\frac{\mathrm{d}\phi_R}{\mathrm{d}t}. \tag{2.12}$$

Straightforward integration then leads to the expression

$$\dot{x}^2 + \dot{y}^2 + \dot{z}^2 = -2\phi_R\left(x, y, z\right) + 2C, \tag{2.13}$$

where C is a constant of integration, usually called the *Jacobi constant* or the *Jacobi integral*. Expressed explicitly, the relation

$$C = \phi_R\left(x, y, z\right) + \frac{1}{2}\left(\dot{x}^2 + \dot{y}^2 + \dot{z}^2\right) \tag{2.14}$$

evaluates the value of the Jacobi constant from the position and velocity of a test particle in the corotating system. This quantity does not change throughout the particle's movement, it is conserved along its trajectory.

2.3 Energy and angular momentum of test particles

The main goal of this thesis is to determine the amount of energy and angular momentum carried away from the system by test particles ejected from the vicinity of the outer Lagrange point L2. To accomplish this objective, we must be able to calculate the values of interest from immediate positions and velocities of the particles in the non-inertial corotating system, which will be obtained by numerical integration of the equations of motion (2.8).

We will consider a test particle positioned at time t at $\mathbf{r_I} = (x_I, y_I, z_I)$ in the inertial reference frame[3] having the immediate velocity $\dot{\mathbf{r}}_\mathbf{I} = (\dot{x}_I, \dot{y}_I, \dot{z}_I)$ with respect to this inertial system. The energy of such particle measured by a stationary inertial observer can be expressed as

$$E\left(\mathbf{r_I}, \dot{\mathbf{r}}_\mathbf{I}, t\right) = \phi_{gravity}\left(\mathbf{r_I}, t\right) + \frac{1}{2}\left(\dot{x}_I^2 + \dot{y}_I^2 + \dot{z}_I^2\right), \tag{2.15}$$

where $\phi_{gravity}\left(\mathbf{r_I}, t\right)$ is the gravitational potential created by the binary system at the location $\mathbf{r_I}$ of the inertial frame of reference. Its value depends on time, as the binary components in this frame orbit around their common centre of mass, so their positions are not fixed. Similarly, the angular momentum of this test particle with respect to the stationary inertial observer will be

$$\mathbf{J}\left(\mathbf{r_I}, \dot{\mathbf{r}}_\mathbf{I}\right) = \left(y_I\dot{z}_I - z_I\dot{y}_I, z_I\dot{x}_I - x_I\dot{z}_I, x_I\dot{y}_I - y_I\dot{z}_I\right). \tag{2.16}$$

[3]A frame of reference where the binary star rotates with the angular velocity $\boldsymbol{\omega}$ with the same units as we used in the corotating frame.

To express the values of energy and angular momentum of a particle with respect to a stationary inertial observer from the particle's immediate position $\mathbf{r} = (x, y, z)$ and velocity $\dot{\mathbf{r}} = (\dot{x}, \dot{y}, \dot{z})$ in the corotating system, we can transform the inertial coordinates into the coordinates used in the corotating frame of reference. Without loss of generality, we will assume that the frames merge at time $t = 0$. The transformation may then be written as

$$\begin{aligned} x_I &= x\cos(\omega t) - y\sin(\omega t), \\ y_I &= x\sin(\omega t) + y\cos(\omega t), \\ z_I &= z, \end{aligned} \tag{2.17}$$

$$\begin{aligned} \dot{x}_I &= \dot{x}\cos(\omega t) - \dot{y}\sin(\omega t) - \omega x\sin(\omega t) - \omega y\cos(\omega t), \\ \dot{y}_I &= \dot{x}\sin(\omega t) + \dot{y}\cos(\omega t) + \omega x\cos(\omega t) - \omega y\sin(\omega t), \\ \dot{z}_I &= \dot{z}. \end{aligned}$$

Substituting (2.17) into (2.15) and (2.16) and carrying out a few basic mathematical adjustments, we are able to write the desired expressions for $E(\mathbf{r}, \dot{\mathbf{r}})$ and $\mathbf{J}(\mathbf{r}, \dot{\mathbf{r}})$. The energy of a test particle that will be measured by a stationary inertial observer, expressed in the units of $a^2\omega^2$, can be computed using the expression

$$\begin{aligned} E(\mathbf{r}, \dot{\mathbf{r}}) = &- \frac{\mu}{\sqrt{(x-1+\mu)^2 + y^2 + z^2}} - \frac{1-\mu}{\sqrt{(x+\mu)^2 + y^2 + z^2}} + \\ &+ \frac{1}{2}\left(\dot{x}^2 + \dot{y}^2 + \dot{z}^2\right) + \frac{1}{2}\left(x^2 + y^2\right) + x\dot{y} - \dot{x}y = \\ = \quad &\phi_R(x, y, z) + \frac{1}{2}\left(\dot{x}^2 + \dot{y}^2 + \dot{z}^2\right) + x^2 + y^2 + x\dot{y} - \dot{x}y, \end{aligned} \tag{2.18}$$

and corresponding third component of its angular momentum[4], in the units of $a^2\omega$, is given by

$$J(\mathbf{r}, \dot{\mathbf{r}}) = x^2 + y^2 + x\dot{y} - \dot{x}y. \tag{2.19}$$

Moreover, comparing these relations with the expression for the Jacobi constant (2.14), we obtain the equality

$$C = E - J, \tag{2.20}$$

implying that the difference between the energy and angular momentum of a particle moving in the xy-plane is conserved along its trajectory.

[4]Later in our work, we will consider only the motion in the plane $z = z_I = 0$. In such situations, because $\dot{z}_I = 0$, both the first and the second components of the angular momentum vector of the particle are equal to zero.

CHAPTER 3

SETTING AND METHODS

To establish the amount of energy and angular momentum that is carried away from the binary system by particles ejected from the vicinity of the L2 point, we investigate trajectories of these particles in the corotating system based on the equations of motion (2.8). We consider only the motion in the plane $z = 0$, since given $z_0 = \dot{z}_0 = 0$, it can be easily seen from the equations (2.8) that the entire trajectory therefore lies in the xy-plane. Moreover, the problem is symmetrical with respect to reflection at the xy-plane, and the equations of motion further imply that the non-trivial entanglement is between the x and y component.

Trajectories of test particles in the xy-plane of the corotating system were obtained by direct numerical integration of the system of equations (2.8a) and (2.8b) using the *scipy.integrate.solve_ivp* function from the *SciPy* library for *Python* (Jones et al. 2001–). We applied the Dormand-Prince method of order 4/5 (*RK45*), which is an explicit method of Runge-Kutta family with adaptive stepsize (Dormand & Prince 1980). It compares the results one would obtain by the Runge-Kutta methods of fourth and fifth order and modifies the stepsize according to the desired consistency between these results. During our computations, relative and absolute tolerances controlling the accuracy were set to 10^{-12}.

We evaluated the trajectories individually for each specific value of initial position and velocity. A necessary input into all of our calculations was the location of the L2 point in the corotating system. The coordinate x_{L2} was established from the implicit equation (2.7) by the secant method using the *scipy.optimize.newton* function. Obtained values of x_{L2} as a function of mass ratio of the system q are visualised in Figure 3.1.

The integration was terminated when one of the following events occurred:

- The particle has crossed the inner equipotential line passing through the L2 point, which implies that it has collided with the common surface of the binary system. An example of such situation is illustrated in the bottom right panel of Figure 3.2.

  To detect this event, we approximated the L2 equipotential curve by a polygon whose vertices were found from the implicit equation

  $$\phi_R(x, y, 0) - \phi_R(x_{L2}, 0, 0) = 0, \tag{3.1}$$

  again using the secant method implemented in the *scipy.optimize.newton* function. Every 0.25 time units (time was measured in the units of ω^{-1}), we

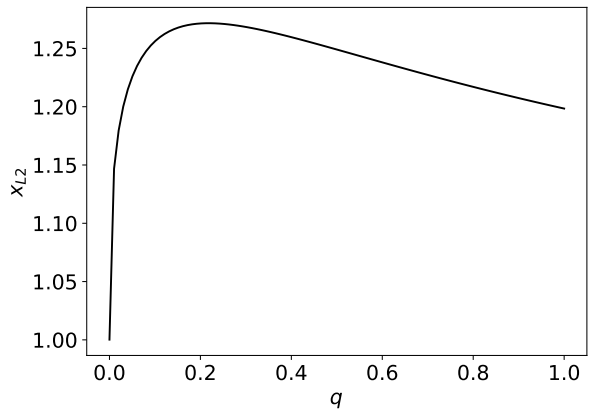

Figure 3.1: The x-coordinate of the second Lagrange point in the corotating system x_{L2} as a function of mass ratio of the binary system q.

evaluated if the particle were located inside the L2 polygon and given a positive result, we interrupted the integration. To construct the polygon and to decide whether it contains a specific point, we used the *matplotlib.path* module from *Matplotlib* library for *Python* (Hunter 2007).

In the situation where the particle falls back into the system no amount of energy or angular momentum is lost from the binary. Thus in such case we did not evaluate the particle's characteristics at the end of the integration, we only marked that a collision had occurred.

- The trajectory has intersected with itself. Considering that the system loses mass by a continuous stream of particles, in such situations the outflow would have struck itself, producing hydrodynamic shocks and invalidating further approximation by test particles. The stream might produce a circular outer ring of matter orbiting around the system, as was considered by Shu et al. 1979; alternatively, under specific initial conditions, it might create a small loop and crash into itself, as we found out during our calculations. Both possibilities are represented in the upper right panel (ring formation) and the bottom left panel (loop) of Figure 3.2.

  To evaluate this condition, after every 0.25 time units we approximated the trajectory of the particle by a line segment connecting the particle's initial and final positions. We then assessed whether this segment crossed with any of the segments constructed in previous steps of the integration. If there was no intersection found, the integration moved over the following 0.25 time units, otherwise the whole process was terminated.

  If the integration was aborted, we took the position and velocity of the particle at the last obtained point of its trajectory before the intersection and using the formulas (2.18) and (2.19), we computed the particle's final values of energy E_f and angular momentum J_f.

- Distance of the particle from system's centre of mass has exceeded 200 a. As the tidal influence of the binary decreases rapidly with growing distance

from the system, energy (2.18) and angular momentum (2.19) usually converge to their final values soon after the particle's ejection. For the same reason, more complicated motion of particles (for example loops as the one we presented in the upper left picture of Figure 3.2), if some, happens close to the system. Consequently, if the particle managed to reach a significant distance from the binary without falling back onto the binary's surface or without intersecting with its previous trajectory, the subsequent path would be quite regular and predictable. Moreover, changes in the values of energy and angular momentum would be minimal and only caused by the inaccuracy of numerical integration.

After the particle reached the distance of 200 a from the centre we terminated the integration and, as in the previously discussed situation, we evaluated the particle's final energy E_f and angular momentum J_f from its last position and velocity.

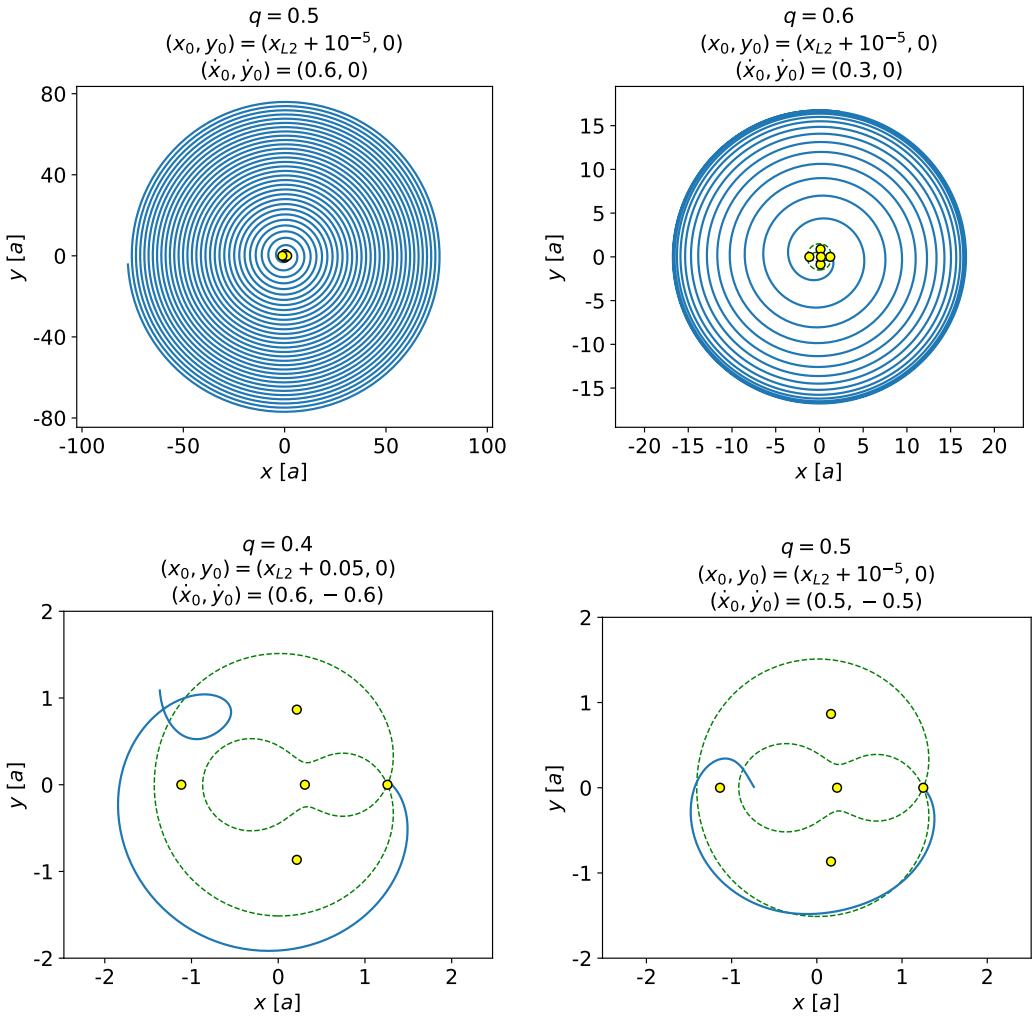

Figure 3.2: Examples of different trajectories of test particles in the corotating system. Trajectories are visualised by the solid blue curves. The dashed green line represents the equipotential line passing through the L2 point and the yellow points mark the locations of the Lagrange points (as in Figure 2.1). The mass ratio q of the binary system and the initial position (x_0, y_0) and velocity $(\dot{x}_0, \dot{y}_0)$ of the trajectory are noted above each picture. The upper right panel is an example of trajectory for a particle that will eventually escape from the system. In the upper right panel, we see the formation of an outer ring of matter orbiting the binary system. The bottom left panel depicts the stream striking itself as it forms a loop, whilst in the bottom right panel, the particle falls back into the binary.

CHAPTER 4

RESULTS AND DISCUSSION

4.1 Comparison with previous results

As was noted in Chapter 1, Shu et al. (1979) established the final values of energy and angular momentum of test particles ejected from the L2 point as a function of mass ratio of the binary system q by numerical integration of the equations of motion (2.8). The particles were ejected from the L2 point, their initial position being $(x_0, y_0, z_0) = (x_{L2}, 0, 0)$, and they were in corotation with the binary system, which means that their initial velocity with respect to the corotating frame of reference was $(\dot{x}_0, \dot{y}_0, \dot{z}_0) = (0, 0, 0)$. The authors noticed two possible outcomes for the particles: they would either become unbound from the binary and escape to infinity, or they would establish a circular orbit around the system. Considering the energy of the particle in its final state, in the first case (unbound) the final energy of the particle would be positive whereas in the second case (bound) the energy of the particle in its final state would be negative.

At first, we applied the method described in Chapter 3 onto the same initial setting as Shu et al. (1979). To avoid the particle falling inside the inner L2 equipotential line at the very beginning of the integration (which could happen as the L2 point is a saddle point), its initial position was set outwards from the L2 point in the x direction by 10^{-5}. Initial conditions for the integration were thus set to $(x_0, y_0) = (x_{L2} + 10^{-5}, 0)$ and $(\dot{x}_0, \dot{y}_0) = (0, 0)$. Our results and the values received by Shu et al. (1979) are visualised in Figure 4.1.

In both cases, the final energy increases from negative values rapidly for small mass ratios up to the point where it crosses zero around $q = 0.064$. After, the rising slows down and it ceases completely between $q = 0.2$ and $q = 0.3$, where the values of final energy start decreasing slowly at approximately constant rate. From our calculations, we found the maximum energy of 0.075 at $q = 0.246$. As the mass ratio approaches 1, the relation passes again into negative values. According to Shu et al. (1979), this happens at $q = 0.78$, however our calculations imply that the second zero-crossing is situated at $q = 0.792$ (see the left bottom panel of Figure 4.1).

The difference between our results rounded off to three decimal places and the values obtained by Shu et al. (1979) does not exceed 0.002. Mostly (for 9 out of 14 q), the energies computed by us (with rounding) are 0.001 higher than those reported by Shu et al. (1979). However, as the authors do not specify the details of their integration, we are unable to determine the precision of their results and

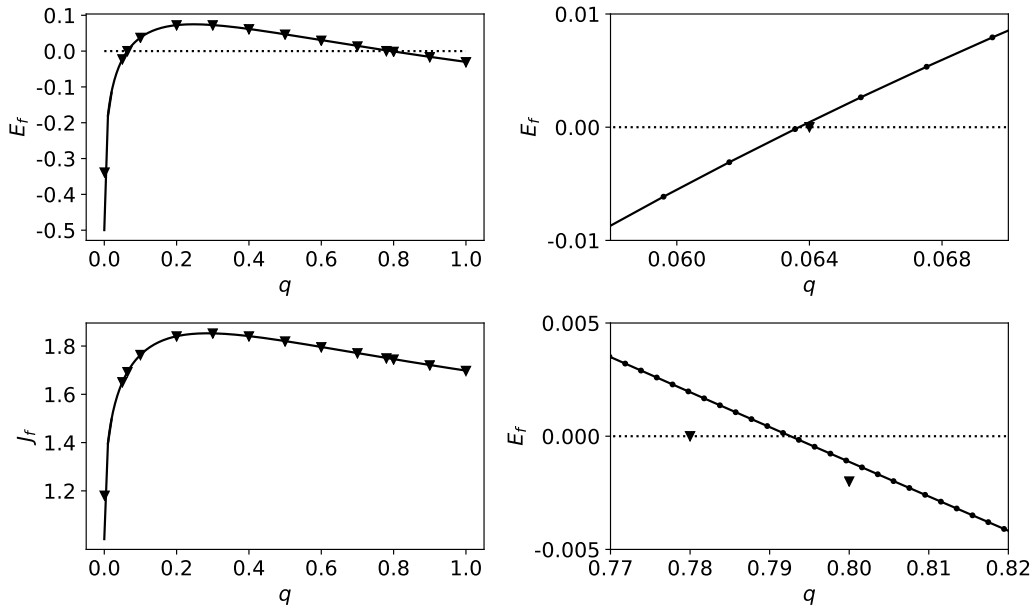

Figure 4.1: Final values of energy E_f and angular momentum J_f for particles ejected from the L2 point as a function of mass ratio of the binary components q. The particles were initially in corotation with the system. We compare our results for initial conditions set to $(x_0, y_0) = (x_{L2} + 10^{-5}, 0)$ and $(\dot{x}_0, \dot{y}_0) = (0, 0)$ (lines with points representing specific values), with the results obtained by Shu et al. (1979) (triangles). Pictures on the left depict the relation in full range of q while panels on the right are close-ups of the regions where E_f crosses zero.

to identify the reason for this disparity.

4.2 Relaxing the corotation at the L2 point

Our first goal was to investigate the behaviour of particles ejected from the L2 point with non-trivial initial velocity with respect to the corotating system. For different directions of initial velocity, we evaluated the relations between the final values of energy and angular momentum, the mass ratio of the binary system and the magnitude of initial velocity. To obtain the figures presented in this section, we split both their axes into 200 linearly spaced points and we coloured every pixel according to the computed value of energy or angular momentum.

4.2.1 Initial velocity in the x-direction

We started with the particles having initial velocity of magnitude v_x in the positive direction of x-axis in the corotating system. Initial conditions for the integration were $(x_0, y_0) = (x_{L2} + 10^{-5}, 0)$ and $(\dot{x}_0, \dot{y}_0) = (v_x, 0)$. Initial values of energy and angular momentum E_i and J_i, their final values E_f and J_f obtained by the integration and also the differences $\Delta E = E_f - E_i$ and $\Delta J = J_f - J_i$ can be seen in Figure 4.2.

Concentrating on the middle left panel illustrating the final energy, we can see that for $v_x = 0$, obtained results are in accord with section 4.1. However, as

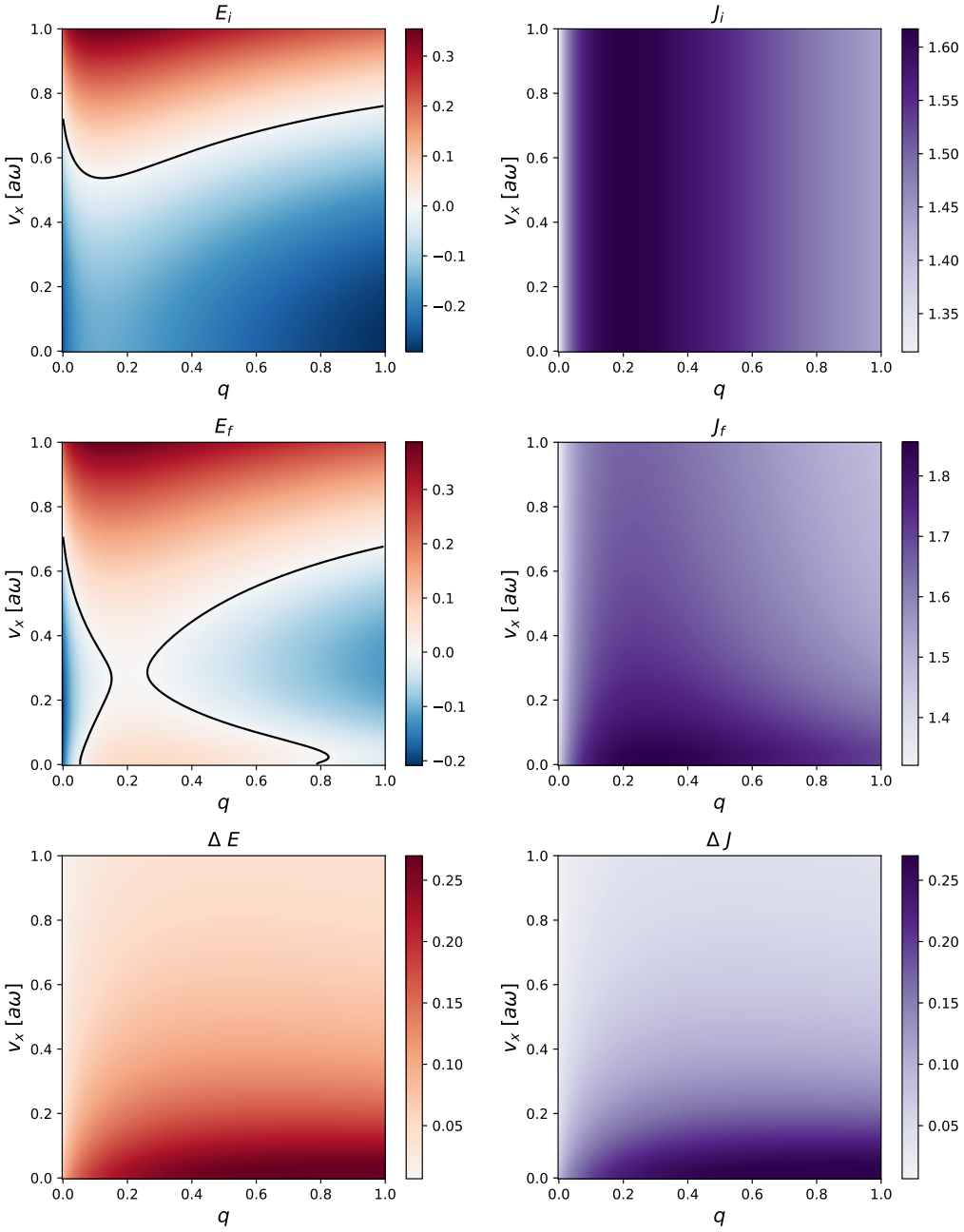

Figure 4.2: Initial and final values of energy and angular momentum and their differences as a function of binary mass ratio q for particles ejected from the L2 point having initial velocity v_x in the positive direction of x-axis. Initial conditions for integration were $(x_0, y_0) = (x_{L2} + 10^{-5}, 0)$ and $(\dot{x}_0, \dot{y}_0) = (v_x, 0)$. The black line depicts the zero energy contour.

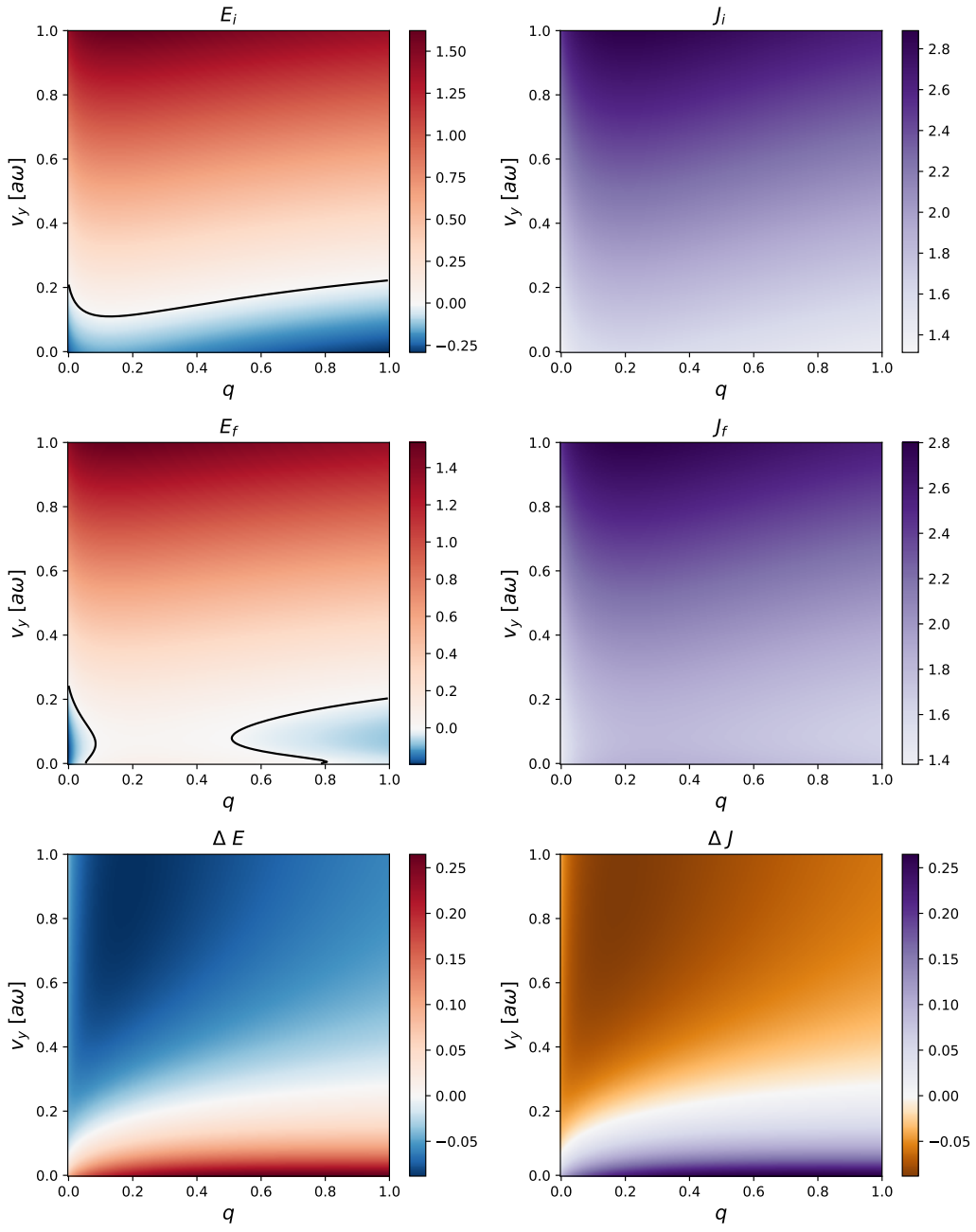

Figure 4.3: Initial and final values of energy and angular momentum and their differences as a function of binary mass ratio q for particles ejected from the L2 point having initial velocity v_y in the positive direction of y-axis. Initial conditions for integration were $(x_0, y_0) = (x_{L2} + 10^{-5}, 0)$ and $(\dot{x}_0, \dot{y}_0) = (0, v_y)$. The black line depicts the zero energy contour.

the magnitude of initial velocity increases, the range of mass ratios for which the particle escapes the system shrinks gradually. The smallest range, approximately from $q = 0.15$ to $q = 0.28$, is reached around $v_x = 0.3$. After that, further increase in velocity's magnitude enlarges the range of mass ratios leading to positive final energy, and if the velocity surpasses 0.7, the particle would stay bound only in the systems with extremely small q.

Moreover, the bottom panels displaying the differences in energy and angular momentum (which are identical because of the relation (2.20)) show that these values are always positive and they decrease with increasing magnitude of velocity. Thus in this setting the particle's energy and angular momentum always rise under the system's influence. This may be explained by the fact that in the inertial frame of reference, the particle lags behind the system. Some of the system's angular momentum is therefore transferred to the particle to accelerate its movement. Angular momentum of the particle increases, and because of the relation (2.20), so does the particle's energy. However, if the particle has higher magnitude of initial velocity, it will distance itself from the system more quickly. This limits the system's influence on the particle to a shorter time period, explaining the decline in the differences as the velocity grows.

4.2.2 Initial velocity in the y-direction

Next we considered particles ejected in the direction of y-axis in the corotating system, with initial conditions $(x_0, y_0) = (x_{L2} + 10^{-5}, 0)$ and $(\dot{x}_0, \dot{y}_0) = (0, v_y)$. Values of E_i, J_i, E_f, J_f and ΔE, ΔJ for positive v_y are visualised in Figure 4.3.

Structure on the middle left panel, which displays the final energy, is similar to the one we established for the velocity pointing in the x-direction, although it is compressed into lower values of velocity's magnitude. Again, at $v_y = 0$ the results overlap with those from section 4.1, and with growing v_y the range of mass ratios for which the particle becomes unbound from the system shrinks. Its minimum is attained around $v_y = 0.1$, where only the systems between $q = 0.1$ and $v_y = 0.5$ are able to throw the particle into infinity. After that point, the range widens again with increasing v_y and above the value of $v_y = 0.25$, all particles escape from the system regardless of its mass ratio.

As we can see from the pictures depicting the differences between final and initial values of energy and angular momentum (bottom panels), for small magnitudes v_y the particle gains energy and angular momentum along its trajectory. However, as v_y grows the differences become increasingly smaller and they gradually pass into negative values, meaning that the particle is losing energy and angular momentum. Same explanation as we proposed above applies onto small values of v_y – the particle lags behind the system, which is trying to accelerate it by transfer of angular momentum. But if the particle's initial velocity is sufficiently big, the roles in the considered scenario will be reversed. The particle will get ahead of the system and the system will try to decelerate it. Therefore it will be the particle transferring its angular momentum to the system.

Additionally, ejecting the particle from the L2 point in the negative direction of y-axis leads to collisions with the binary for all mass ratios in wide range of magnitudes v_y. However, ring formation starts to emerge around $v_y = 2.0$, and for magnitudes higher than $v_y = 2.5$, most particles escape from the system with

positive energy.

4.3 Ejection from corotation from the surroundings of the L2 point

In our next step we evaluated final values of energy and angular momentum for particles ejected from the neighbourhood of the L2 point from corotation with the binary system.

4.3.1 Dislocation along x-axis and y-axis

At first we studied the evolution of final energy and angular momentum as a function of mass ratio as the initial position of the particles shifted from the L2 point along x-axis and y-axis. We present our results for displacements in the x-direction Δx and y-direction Δy in Figure 4.4 and Figure 4.5, respectively. Again, to obtain these pictures we generated 200 linearly spaced values along both axes and coloured each pixel according to the computed value of energy or angular momentum.

From the middle left panel of Figure 4.4, illustrating the final energy, we can see that the range of mass ratios for which the particle escapes the system narrows as we move further from the L2 point along the x-axis and then it begins to widen again. The smallest range is attained around $\Delta x = 0.025\ a$, bounded approximately by values $q = 0.05$ and $q = 0.065$. However, if the particle begins its motion further that $\Delta x = 0.125\ a$ from the L2 point, it will become unbound from the system regardless of its mass ratio.

Moreover, in accordance with the explanation proposed in section 4.2, bottom panels of Figure 4.4 depicting the differences between particle's initial and final energy and angular momentum show that these values are always positive. The particle, ejected from the L2 point or further with no initial velocity with respect to the corotating system always falls behind the binary and thus gains angular momentum and energy at the expense of the system.

The structures represented in Figure 4.5 are more complicated. If we shift the initial position slightly upwards from the L2 point, in the positive direction of y-axis, the particle falls into the binary regardless of the system's mass ratio. However, the middle left panel illustrates that as the initial distance from the L2 point grows, in systems with relatively small q the particle eventually forms a ring around the binary. Moreover, for bigger Δy a range of q for which the particle escapes to infinity appears. On the other hand, moving the launching point downwards from the L2 point, in the negative direction of y-axis, at first narrows slightly the range of q for which the particle becomes unbound and then, as the distance increases more, this range widens considerably. After the distance exceeds $\Delta y = -0.15\ a$, only the systems with extremely small mass ratio $q < 0.02$ are unable to throw the particle into infinity.

Particle ejected from underneath the L2 point will always gain energy and angular momentum from the binary because it lags behind the system. Contrarily, in the left upper corner of bottom panels in Figure 4.5 we can notice that for positive Δy, there is a band representing initial configurations where the particle's

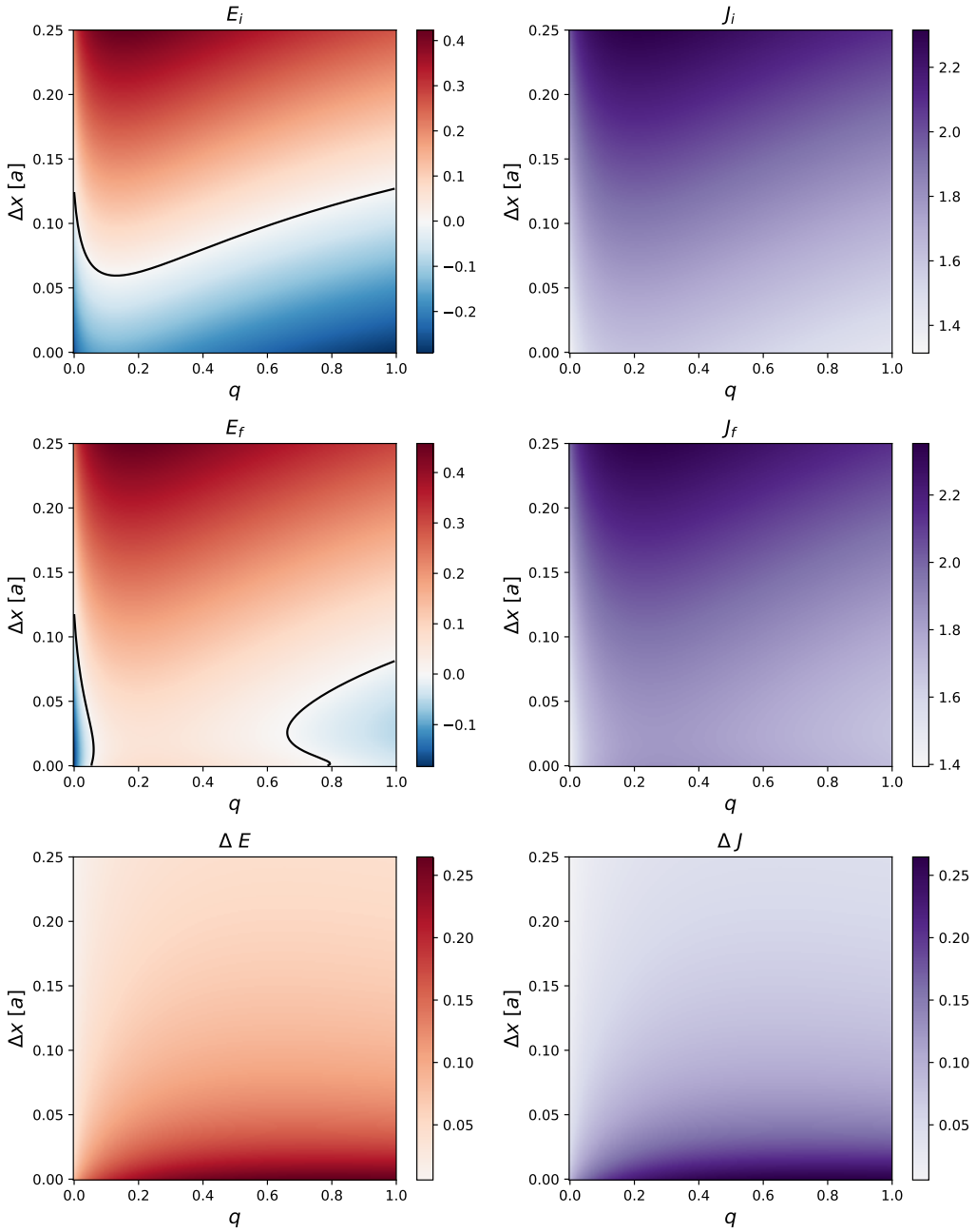

Figure 4.4: Initial and final values of energy and angular momentum and their differences as a function of binary mass ratio q for particles ejected from initial position $(x_0, y_0) = (x_{L2} + \Delta x, 0)$ with initial velocity $(\dot{x}_0, \dot{y}_0) = (0, 0)$. The black line depicts the zero energy contour.

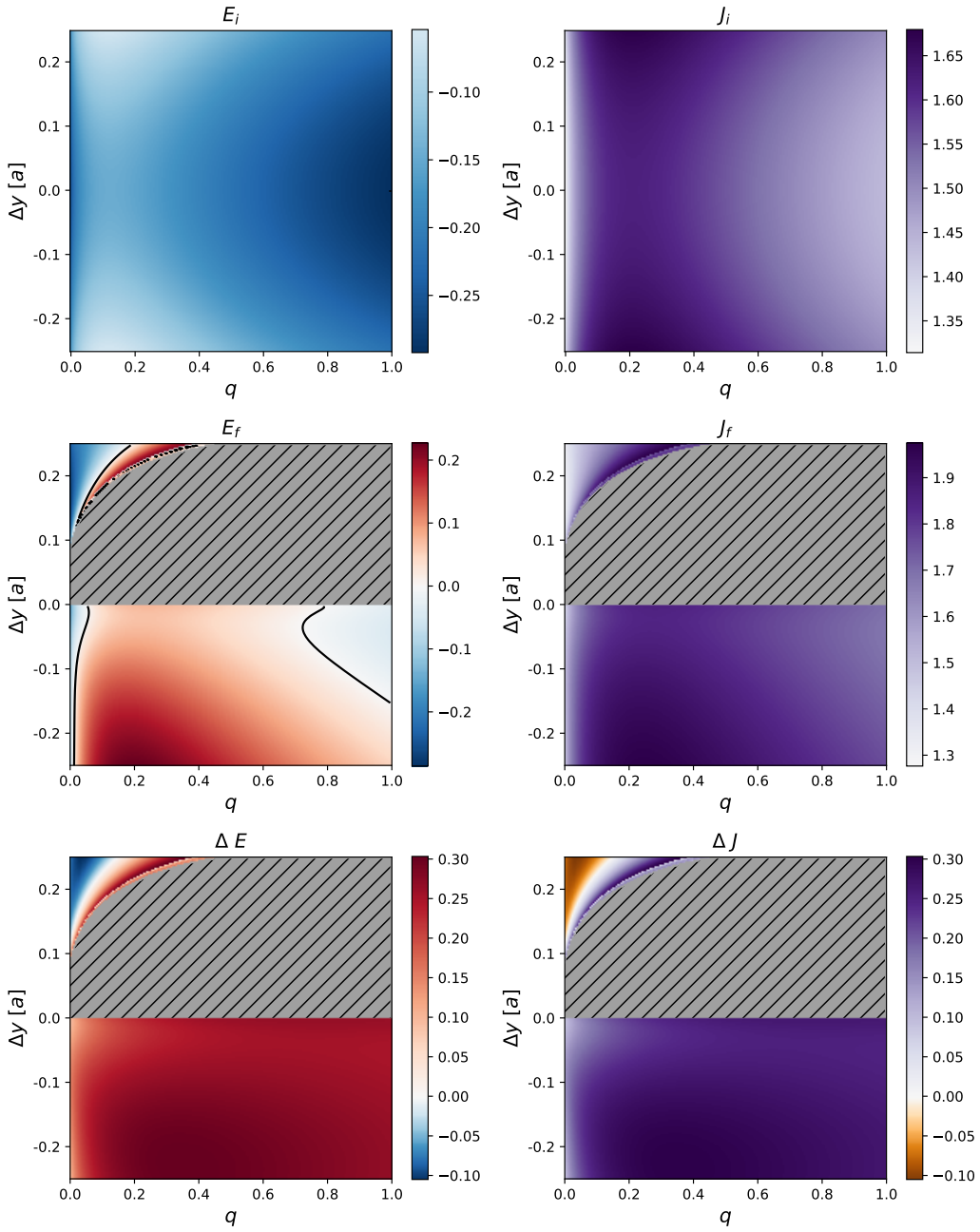

Figure 4.5: Initial and final values of energy and angular momentum and their differences as a function of binary mass ratio q for particles ejected from initial position $(x_0, y_0) = (x_{L2}, \Delta y)$ with initial velocity $(\dot{x}_0, \dot{y}_0) = (0, 0)$. The black line depicts the zero energy contour. The hatched part marks those values for which the particle fell back into the binary system (see the bottom right panel in Figure 3.2)

energy and angular momentum decrease along its trajectory. Additionally, this band starts at small q and includes more values of mass ratio as Δy grows. However, it is simply a consequence of different relevant scales for various q. In a binary with small mass ratio, particle positioned more than $\Delta y = 0.1\ a$ above the L2 point will be moving ahead of the binary, losing energy and angular momentum. To achieve the same for systems whose mass ratio is higher, initial distance between the particle and the L2 point would have to be considerably bigger.

For those combinations of parameters which are located at the boundary of the gray hatched area the trajectory formed a loop and the integration was terminated at the point of intersection. This is the reason behind the apparent discontinuities in the final values and differences displayed in Figure 4.5.

4.3.2 General initial position with fixed mass ratio

Secondly, we chose a specific value of q and we created a grid centered around the L2 point containing 100×100 points (actual physical dimension was adjusted to q). Each point of the grid was then used as an initial position for a test particle which we ejected from corotation. However, we did not initiate the integration if the point lay inside the inner part of the equipotential line passing through the L2 point.

We considered three values of q: small $q = 0.05$, intermediate $q = 0.5$ and big $q = 0.95$. To visualise our results, we coloured every pixel corresponding to a specific initial location according to the computed value of energy. Pictures depicting initial and final energies and their differences for all three values of mass ratio are presented in Figure 4.6[1].

Noticing the pictures displaying the final energy (middle row), we can see that they are in accordance with previous results discussed in section 4.3.1 (Figure 4.4, displacement along x-axis, and Figure 4.5, displacement along y-axis,). For $q = 0.05$ and $q = 0.95$, ejecting the particle from close proximity of the L2 point leads to it establishing a circular orbit around the binary; furthermore, the distance from the L2 point necessary for the particle to be thrown to infinity is bigger for the bigger mass ratio $q = 0.95$ in both x and y-direction. Contrarily, we see that for $q = 0.5$, the particle ejected from the vicinity of the L2 point will become unbound from the system.

Moreover, the L2 equipotential line is framed by pronounced areas from which the particle falls back into the binary system (see the bottom right panel in Figure 3.2). These are situated both upwards and downwards from the L2 point, and the upper area is slightly wider than the one below.

[1]From this point forward, we display only the energy and not the angular momentum as ΔJ is identical to ΔE and the information about whether the particle escapes from the system or stays bound to it is in the value of E_f.

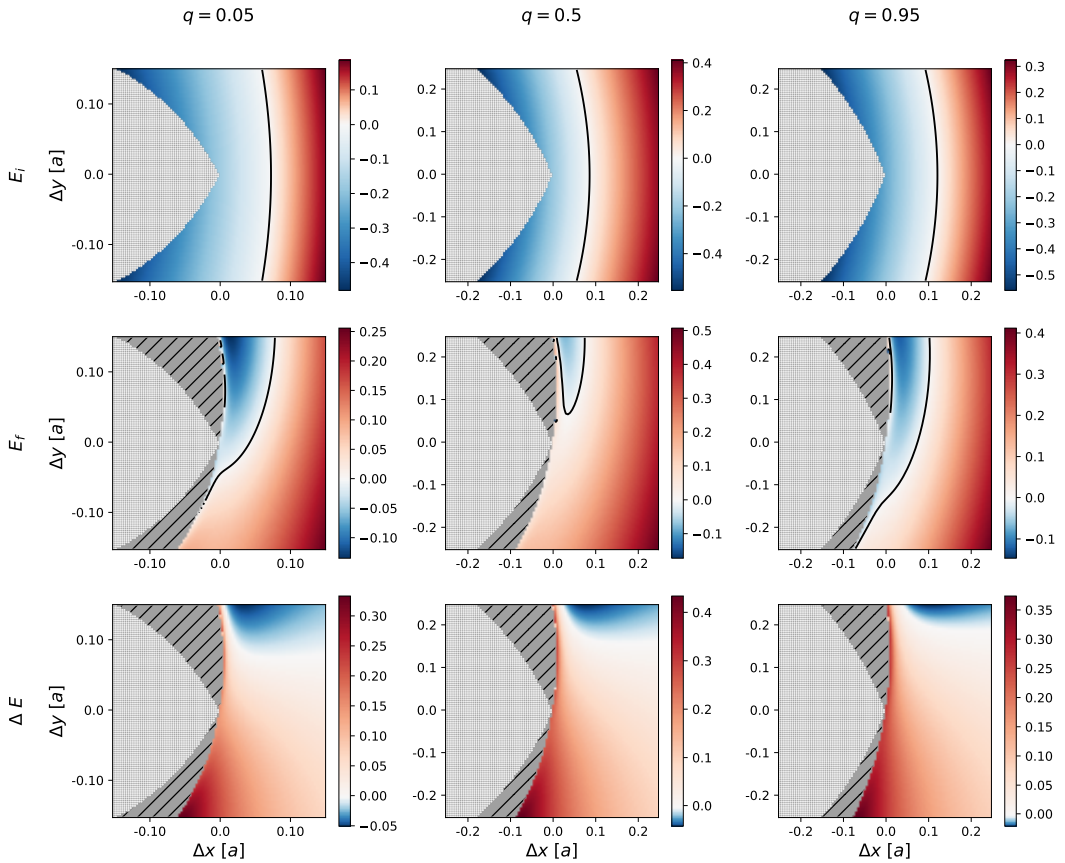

Figure 4.6: Initial and final values of energy and their differences for particles ejected from $(x_0, y_0) = (x_{L2} + \Delta x, \Delta y)$ with initial velocity $(\dot{x}_0, \dot{y}_0) = (0, 0)$. Left column contains results for $q = 0.05$, middle column results for $q = 0.5$ and in the right column, we present results for $q = 0.95$. Black curves depicted are zero energy contours. Hatches mark the parts of parameter space where the particle collided with the inner L2 equipotential line (see the bottom right panel in Figure 3.2) and the shape dotted with white points represents initial positions lying inside the inner L2 equipotential line.

4.4 Ejection in radial direction from the surroundings of the L2 point

Using the same arrangement as in section 4.3.2 we evaluated final energies of particles ejected from general locations in the vicinity of the L2 point in radial direction. Releasing the particle from (x_0, y_0), its initial velocity was set to

$$(\dot{x}_0, \dot{y}_0) = \frac{v_0}{\sqrt{x_0^2 + y_0^2}} (x_0, y_0) , \tag{4.1}$$

where v_0 specified the velocity's magnitude. We present our results in Figure 4.7.

Comparing these results with final energies depicted in Figure 4.6, where the particles initiated from corotation, we note that given radial initial velocity, the areas from which the particles fall into the binary recede backwards from the L2 point, further away as the velocity's magnitude increases. More particles are able to fly away from the system (either forming a ring or escaping to infinity), because the initial kick in radial direction overcomes the Coriolis force that would otherwise pull the particle into the binary.

At the same time, as the magnitude grows the space with negative final energy advances downwards and recedes towards the L2 point and further away. For $q = 0.05$ and $q = 0.95$ this retreat will eventually leave the closest surroundings of the L2 point with positive final energy. On the other hand, for $q = 0.5$, the L2 point lies at first in the part of parameter space with positive final energy and as the velocity's magnitude grows it is encompassed by the space with negative final energy. However, if the magnitude is big enough, all the particles ejected from the proximity of the L2 point would eventually be able to escape from the system to infinity, too.

Considering that at the L2 point the initial velocity pointed in the positive direction of x-axis, these results are compatible with those illustrated in Figure 4.2. For $q = 0.05$ the particle from the L2 point will escape from the system if v_x is bigger than 0.5 $a\omega$ and similarly for $q = 0.95$, where the smallest necessary velocity is a little bit under 0.7 $a\omega$. However, considering $q = 0.5$, the particle escapes if $v_x < 0.15\ a\omega$ or otherwise if $v_x > 0.55\ a\omega$.

4.5 Ejection in tangential direction from the surroundings of the L2 point

Finally, we studied the behaviour of particles ejected from general positions near the L2 point with velocities pointing in tangential direction. If the particle's initial position was (x_0, y_0), its initial velocity was calculated from the relation

$$(\dot{x}_0, \dot{y}_0) = \begin{cases} \frac{v_0}{\sqrt{x_0^2+y_0^2}} (-y_0, x_0) & \text{if } y_0 > 0 \\ (0, v_0) & \text{if } y_0 = 0 \\ \frac{v_0}{\sqrt{x_0^2+y_0^2}} (y_0, -x_0) & \text{if } y_0 < 0 \end{cases} , \tag{4.2}$$

where v_0 determined the velocity's magnitude. The particle was ejected in the direction of rotation if $v_0 > 0$, contrarily if $v_0 < 0$ the initial velocity pointed in the direction opposite to system's rotation.

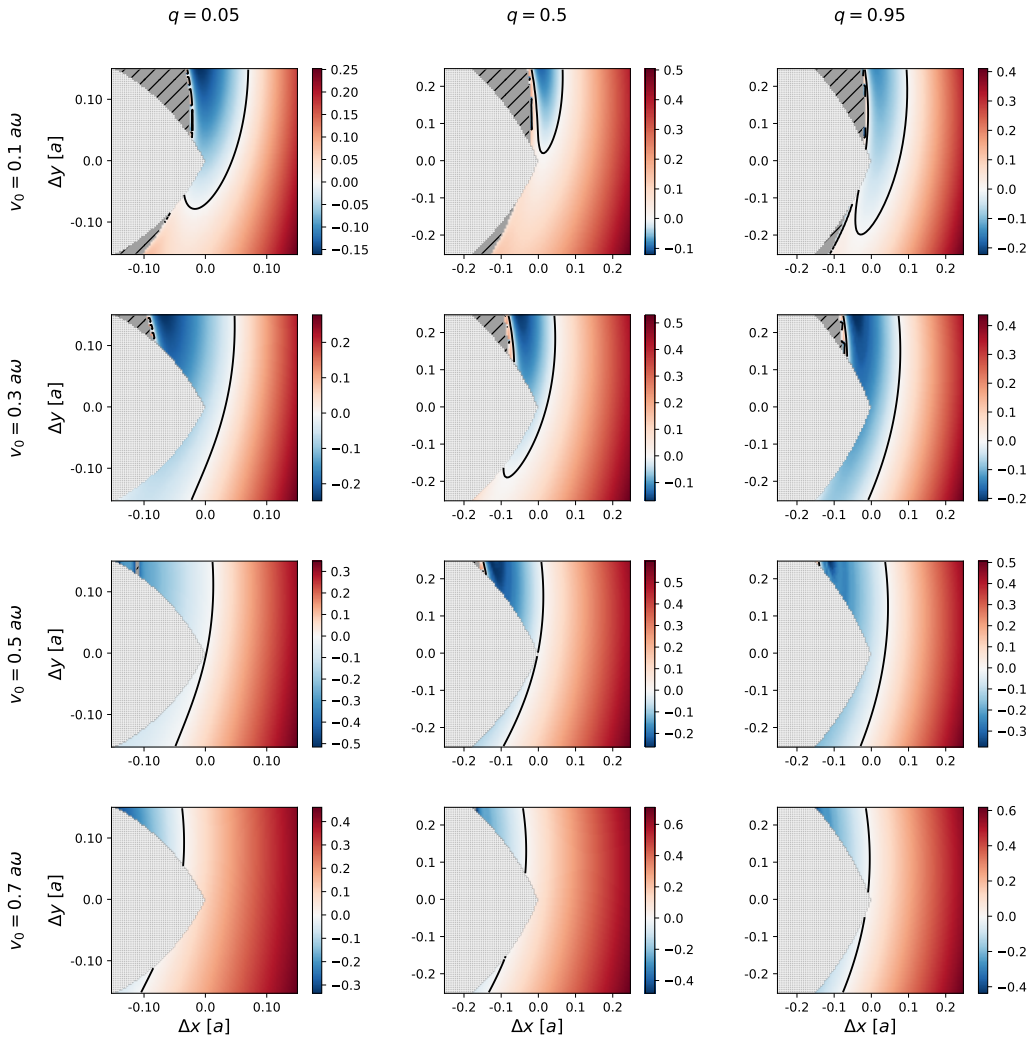

Figure 4.7: Final energy for particles ejected from $(x_0, y_0) = (x_{L2} + \Delta x, \Delta y)$ with initial velocity in the radial direction established by relation (4.1). In the first row, initial velocity's magnitude was set to $v_0 = 0.1\ a\omega$, in the second row $v_0 = 0.3\ a\omega$, in the third row we used $v_0 = 0.5\ a\omega$ and in the last row $v_0 = 0.7\ a\omega$. Left column contains results for $q = 0.05$, middle column results for $q = 0.5$ and in the right column, we present results for $q = 0.95$. Black curves are zero energy contours. Hatches mark the parts of parameter space where the particle collided with the inner L2 equipotential line (see the bottom right panel in Figure 3.2) and the shape dotted with white points represents initial positions lying inside the inner L2 equipotential line.

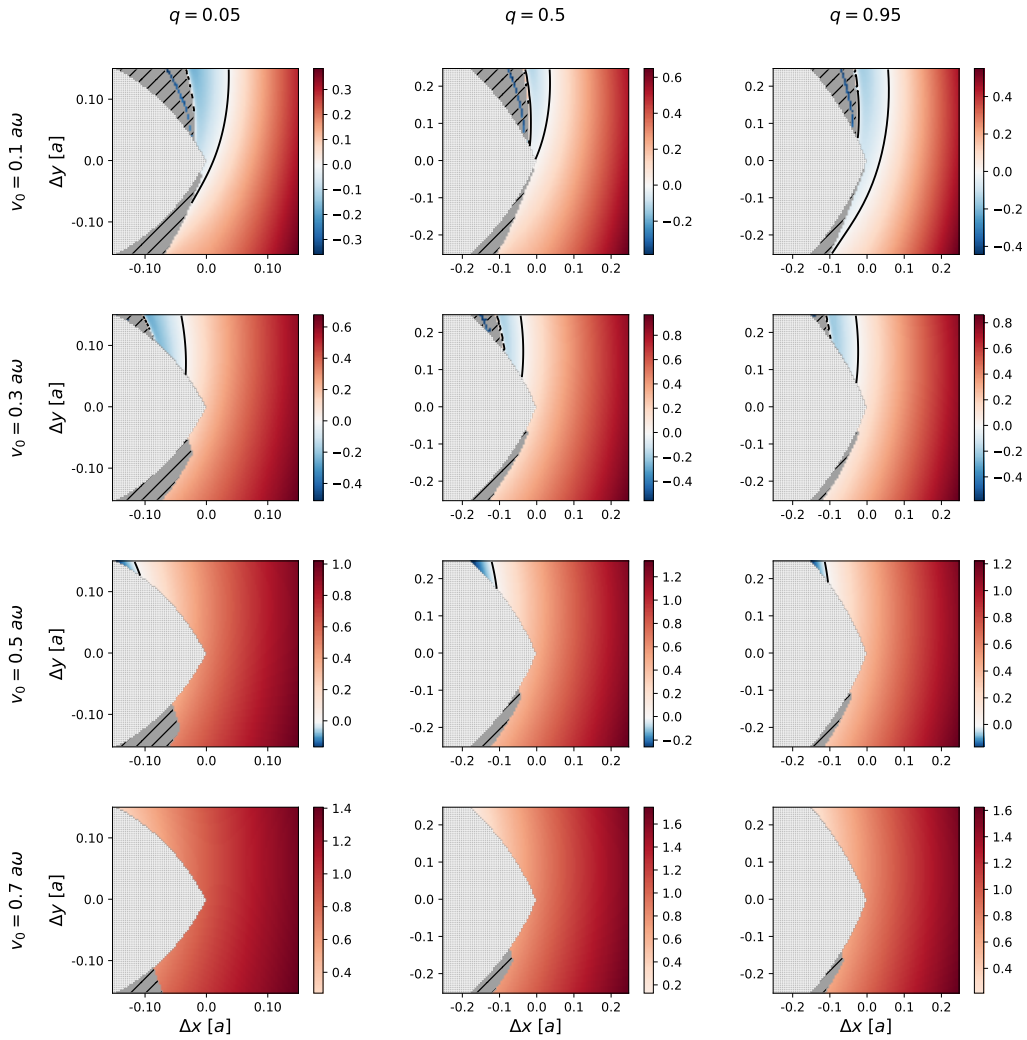

Figure 4.8: Final energy for particles ejected from $(x_0, y_0) = (x_{L2} + \Delta x, \Delta y)$ with tangential initial velocity in the direction of system's rotation, established by relation (4.2). In the first row, initial velocity's magnitude was $v_0 = 0.1\ a\omega$, in the second row $v_0 = 0.3\ a\omega$, in the third row we used $v_0 = 0.5\ a\omega$ and in the last row $v_0 = 0.7\ a\omega$. Left column contains results for $q = 0.05$, middle column results for $q = 0.5$ and in the right column, we present results for $q = 0.95$. Black curves are zero energy contours. Hatches mark the parts of parameter space where the particle collided with the inner L2 equipotential line (see the bottom right panel in Figure 3.2) and the shape dotted with white points represents initial positions lying inside the inner L2 equipotential line.

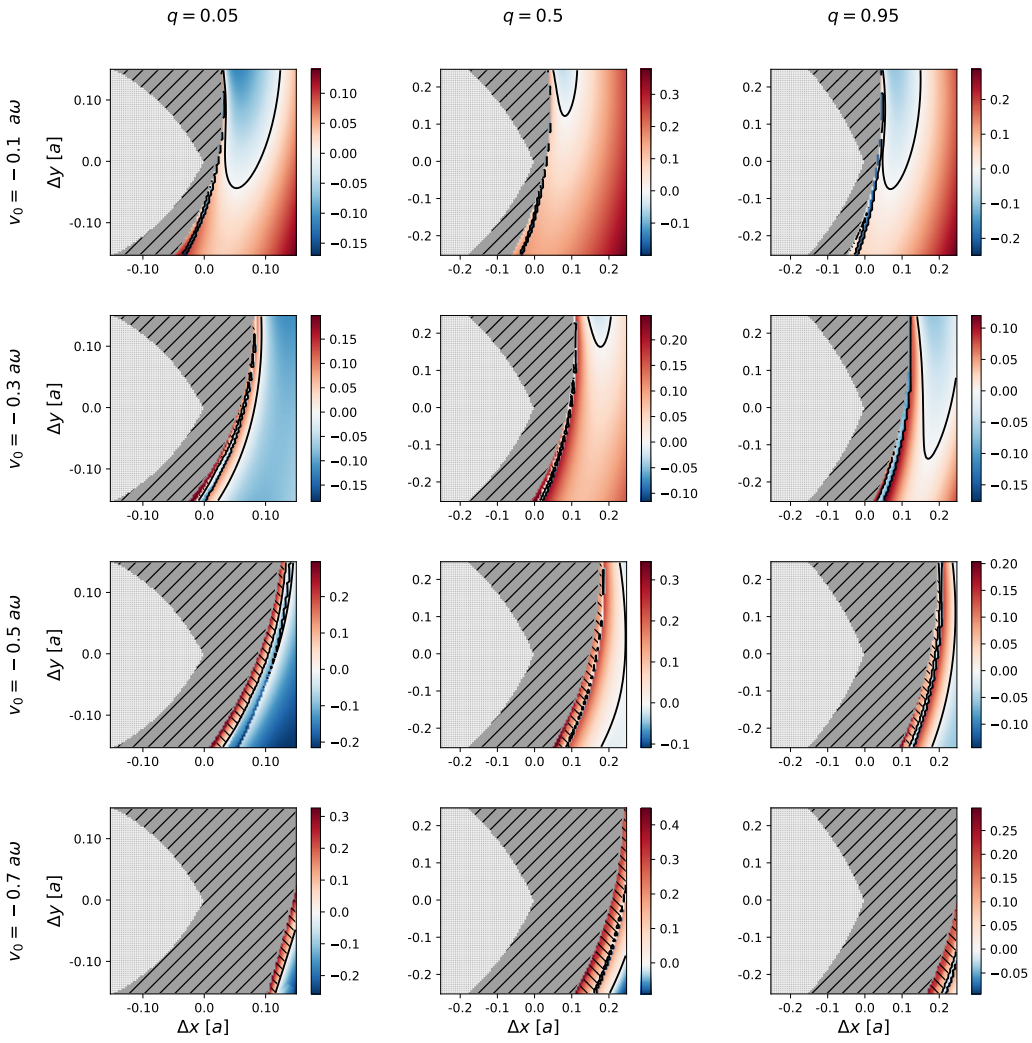

Figure 4.9: Final energy for particles ejected from $(x_0, y_0) = (x_{L2} + \Delta x, \Delta y)$ with tangential initial velocity in the direction opposite to system's rotation, established by relation (4.2). In the first row, initial velocity's magnitude was set to $v_0 = -0.1\ a\omega$, in the second row $v_0 = -0.3\ a\omega$, in the third row we used $v_0 = -0.5\ a\omega$ and in the last row $v_0 = -0.7\ a\omega$. Left column contains results for $q = 0.05$, middle column results for $q = 0.5$ and in the right column, we present results for $q = 0.95$. Black curves are zero energy contours. Hatched gray areas are parts of parameter space where the particle collided with the inner L2 equipotential line (see the bottom right panel in Figure 3.2) and the shape dotted with white points represents initial positions lying inside the inner L2 equipotential line. Hatched areas with positive final energy mark initial locations from which the particle did not escape to infinity because its trajectory formed a loop that terminated the integration (as in the bottom left panel in Figure 3.2), however, at the point of intersection the particle had positive energy.

To compute and visualise our results we used the same arrangement as in section 4.3.2. In Figure 4.8 we present final values of energy for particles ejected in the direction of rotation; final energies for particles ejected in the opposite direction are displayed in Figure 4.9.

Focusing at first on Figure 4.8, we can see that the areas where the particles collided with the binary system recede backwards from the L2 point, similarly as in Figure 4.7 (velocity in radial direction). Analogically to what we proposed in section 4.4, if we eject the particle with some non-trivial velocity in the direction of rotation, the Coriolis force will not be able to spiral the trajectory into the system, and the particle will be able to fly away from the binary.

Additionally, the space with negative final energy narrows as the velocity's magnitude increases. By $v_0 = 0.3$, it is restricted into the area above the L2 equipotential line for all three values of q and with growing magnitude it recedes further backwards from the L2 point. At the L2 point, the initial velocity points in the positive direction of y-axis; at this point the final states of particles for different v_0 are in accordance with those presented in Figure 4.3 for corresponding v_y.

In the first two rows we can note a thin line of initial positions with negative final energy passing through the upper area where the particles collided with the system. Trajectories of particles initiated in these locations formed a loop (as in bottom left panel of Figure 3.2) before they crossed the inner L2 equipotential line. Our integrator thus evaluated as final energy the energy that the particle had at the point of intersection.

From Figure 4.9 we can see that if we eject the particle in the direction opposite to system's rotation, the outcome will be completely different from all previous results. Mainly we note that the areas from which the particles collided with the inner L2 equipotential line are widening as the velocity's magnitude increases. More and more particles are pulled towards the binary and fall inside, consequently not leaving the system at all.

Moreover, trajectories of particles ejected from the boundaries of gray hatched areas form loops as a result of Coriolis acceleration. In such cases, values of energy displayed in Figure 4.9 are evaluated before the trajectory crosses itself. This is the origin of distinctive thin lines with negative final energy visible in most of the pictures. Furthermore, we detected situations in which the particle had positive final energy at the point of intersection. We distinguish them from those particles that escaped from the system to infinity by hatches.

4.6 Dependence on initial setting

Whilst investigating the motion of particles ejected from the L2 point with velocity pointing under 45 degrees into the fourth quadrant we obtained an interesting result highlighting the complexity of the task at hand. We ejected the particle from $(x_0, y_0) = (x_{L2} + 10^{-5}, 0)$ with initial velocity $(\dot{x}_0, \dot{y}_0) = (v_0, -v_0)$ and we evaluated the energy in its final state as a function of system's mass ratio q and v_0. Obtained values are displayed in Figure 4.10.

The structure of the relation between final energy, mass ratio of the system and magnitude of the initial velocity (equal to $\sqrt{2}v_0$) is quite complicated. For higher values of q and small v_0 the particles tend to fall into the binary system;

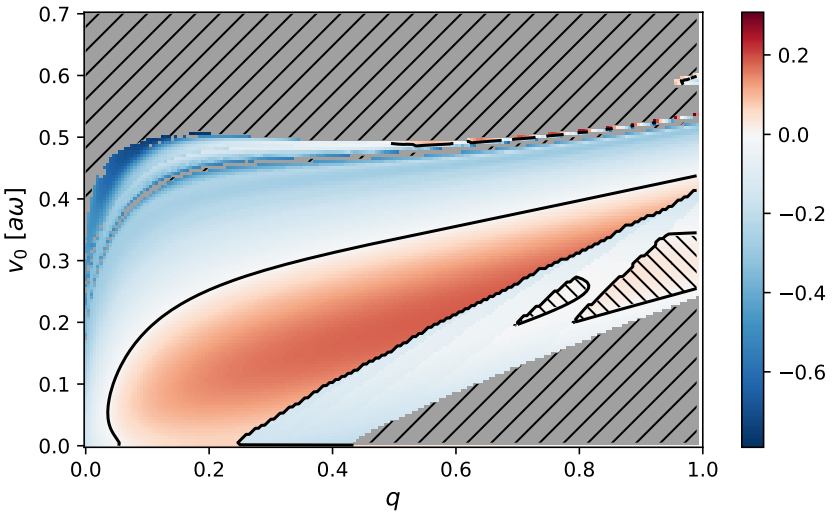

Figure 4.10: Final energy for particles ejected from $(x_0, y_0) = (x_{L2} + 10^{-5}, 0)$ with initial velocity $(\dot{x}_0, \dot{y}_0) = (v_0, -v_0)$. The black line represents the zero energy contour. Grey hatched areas mark those parts of parameter space where the particle collided with the inner L2 equipotential line (see the bottom right panel in Figure 3.2) and hatches over areas with positive final energy distinguish the situations in which the trajectory intersected with itself from the cases in which the particle managed to escape to infinity (positive final energy without hatches).

however, as the magnitude grows their trajectories start forming loops, implying the occurrence of hydrodynamic shocks in the mass loss stream. Some of the particles even had positive energy just before the collision, we single out those cases by hatches.

Moreover, we can see a pronounced jump from conditions leading to loop formation to those for which the particle managed to escape from the system to infinity. After, as the velocity's magnitude increases the final energy evolves continuously, nevertheless between $v_0 = 0.4$ and $v_0 = 0.6$ (slightly lower for the smallest values of q) we observe a strong dependence of the final state on input parameters. While in some cases the particle collides with the binary system, in others its trajectory intersects while the particle has mostly negative, but sometimes even positive energy. This disparities are mostly caused by the geometry and the setting of the problem. For example, under some favorable conditions the particle may approach one of the L3, L4 or L5 points during its movement; and as the Roche potential varies considerably around these points, a slight change in the initial setting might significantly modify the particle's trajectory.

CHAPTER 5

CONCLUSION

In this thesis we studied the loss of mass and angular momentum from binary systems that may arise when the common envelope of a contact binary exceeds over the outer Lagrange point. In all of the previous works, the L2 mass loss was studied with the assumption of the matter being initially in corotation with the system and escaping directly from the L2 point. However, using test particles as a simple approximation, we examined basic characteristics of the mass loss stream if the matter initiated from the surroundings of the L2 point and, moreover, if it was not necessarily initially corotating with the binary.

For this purpose we investigated the behaviour of test particles ejected from the binary from the proximity of the L2 point under general initial conditions. We focused mainly on their final states, that is whether they fell back into the system or if they were able to escape to infinity, or else if they stayed bound to the binary, forming a ring of orbiting matter, and finally if their trajectory otherwise intersected with itself, which would lead to hydrodynamic shocks. Moreover, we evaluated the amount of energy and angular momentum that the particles carried away from the system.

As a first step, we verified the results of Shu et al. (1979) by establishing the final values of energy and angular momentum as a function of mass ratio q of the binary system for particles ejected from the L2 point from initial corotation. We concluded that particles are thrown to infinity by systems with $0.064 < q < 0.792$, whereas if $q < 0.064$ or $q > 0.792$, particles stay bound to the binary, establishing a circular orbit around the system.

Secondly, we studied the ejection of particles from the L2 point in the direction of x-axis and y-axis. We computed the final energy and angular momentum as a function of velocity's magnitude and mass ratio of the system and also the difference between their final and initial values. Particle gained energy and angular momentum at the expense of the binary if it was lagging behind the system because the system was trying to accelerate its motion. On the other hand, if the particle got ahead of the binary after its ejection, it lost some of its initial energy and angular momentum, as the system was trying to decelerate it.

Next, we investigated the influence of particle's initial location on its final state when the particle started its motion from corotation. We evaluated how the final energy and angular momentum evolve as a function of q if we additionally shift the particle along x-axis and y-axis. Furthermore, for three fixed values of q — 0.05, 0.5 and 0.95 — we constructed pictures of the area surrounding the L2 point indicating the final state of the particle and its energy for each depicted

initial location. We noted that particles initiated from wide areas around the L2 equipotential line are not able to fly away from the system at all as they fall into the binary due to Coriolis acceleration. However, for all three values of q we found a set of initial positions from which the particles escaped from the system to infinity.

Finally, we examined the most general cases where we ejected the particles from a grid of initial positions in the vicinity of the L2 point with some specific initial velocity. We considered three directions for the velocity — radial, tangential in the direction of rotation and tangential in the direction opposite to rotation — and we evaluated final states of particles for $q = 0.05, 0.5, 0.95$ and for various values of velocity's magnitude. For the first two directions of initial velocity, we saw that as the magnitude increases, more particles from the vicinity of the inner L2 equipotential line are able to fly away from the system; moreover that most of the particles will eventually escape from the system to infinity. However, ejecting the particles in the opposite direction of rotation leads to them falling into the system more easily or producing hydrodynamic shocks as their trajectory intersects with itself.

BIBLIOGRAPHY

Abbott, B., Abbott, R., Abbott, T., Abernathy, M., Acernese, F., Ackley, K., Adams, C., Adams, T., Addesso, P., Adhikari, R. et al. (2016*a*), 'GW151226: Observation of gravitational waves from a 22-solar-mass binary black hole coalescence', *Physical Review Letters* **116**(24), 241103.

Abbott, B. P., Abbott, R., Abbott, T., Abernathy, M., Acernese, F., Ackley, K., Adams, C., Adams, T., Addesso, P., Adhikari, R. et al. (2016*b*), 'Observation of gravitational waves from a binary black hole merger', *Physical Review Letters* **116**(6), 061102.

Abbott, B. P., Abbott, R., Abbott, T., Acernese, F., Ackley, K., Adams, C., Adams, T., Addesso, P., Adhikari, R., Adya, V. et al. (2017*a*), 'GW170814: A three-detector observation of gravitational waves from a binary black hole coalescence', *Physical Review Letters* **119**(14), 141101.

Abbott, B. P., Abbott, R., Abbott, T., Acernese, F., Ackley, K., Adams, C., Adams, T., Addesso, P., Adhikari, R., Adya, V. et al. (2017*b*), 'GW170817: Observation of gravitational waves from a binary neutron star inspiral', *Physical Review Letters* **119**(16), 161101.

Belczynski, K., Holz, D. E., Bulik, T. & O'Shaughnessy, R. (2016), 'The first gravitational-wave source from the isolated evolution of two stars in the 40 – 100 solar mass range', *Nature* **534**(7608), 512.

Danby, J. (1992), *Fundamentals of celestial mechanics*, Richmond: Willman-Bell, 2nd ed.

De Loore, C. & De Greve, J. (1992), 'Evolutionary sequences for binary stars in the mass range 9 to 40 solar masses', *Astronomy and Astrophysics Supplement Series* **94**, 453–478.

Dormand, J. R. & Prince, P. J. (1980), 'A family of embedded Runge-Kutta formulae', *Journal of computational and applied mathematics* **6**(1), 19–26.

Eggleton, P. (2006), *Evolutionary processes in binary and multiple stars*, Vol. 40, Cambridge University Press.

Flannery, B. P. & Ulrich, R. K. (1977), 'On the origin of Centaurus X-3 and related binary X-ray sources', *The Astrophysical Journal* **212**, 533–540.

Giuricin, G. & Mardirossian, F. (1981), 'Some aspects of mass loss and mass transfer in Algol variables', *The Astrophysical Journal Supplement Series* **46**, 1–26.

Harmanec, P. & Brož, M. (2011), *Stavba a vývoj hvězd*, Matfyzpress.

Heger, A., Fryer, C., Woosley, S., Langer, N. & Hartmann, D. H. (2003), 'How massive single stars end their life', *The Astrophysical Journal* **591**(1), 288.

Humphreys, R. M. & Davidson, K. (1994), 'The luminous blue variables: Astrophysical geysers', *Publications of the Astronomical Society of the Pacific* **106**(704), 1025.

Hunter, J. D. (2007), 'Matplotlib: A 2D graphics environment', *Computing In Science & Engineering* **9**(3), 90–95.

Iben, I. & Livio, M. (1993), 'Common envelopes in binary star evolution', *Publications of the Astronomical Society of the Pacific* **105**(694), 1373.

Ivanova, N. (2015), Binary evolution: Roche lobe overflow and blue stragglers, *in* 'Ecology of Blue Straggler Stars', Springer, pp. 179–202.

Ivanova, N., Justham, S., Chen, X., De Marco, O., Fryer, C., Gaburov, E., Ge, H., Glebbeek, E., Han, Z., Li, X.-D. et al. (2013), 'Common envelope evolution: Where we stand and how we can move forward', *The Astronomy and Astrophysics Review* **21**(1), 59.

Jones, E., Oliphant, T., Peterson, P. et al. (2001–), 'SciPy: Open source scientific tools for Python'. `http://www.scipy.org/` (2.6.2018).

Kuiper, G. P. (1941), 'On the interpretation of Beta Lyrae and other close binaries.', *The Astrophysical Journal* **93**, 133.

Lamers, H. J. & Cassinelli, J. P. (1999), *Introduction to stellar winds*, Cambridge university press.

Langer, N. (2012), 'Presupernova evolution of massive single and binary stars', *Annual Review of Astronomy and Astrophysics* **50**.

Linial, I. & Sari, R. (2017), 'Mass-loss through the L2 Lagrange point – application to main -sequence EMRI', *Monthly Notices of the Royal Astronomical Society* **469**(2), 2441–2454.

Livio, M., Salzman, J. & Shaviv, G. (1979), 'The formation of planetary nebulae with close binary nuclei', *Monthly Notices of the Royal Astronomical Society* **188**(1), 1–12.

Lombardi Jr, J. C., Holtzman, W., Dooley, K. L., Gearity, K., Kalogera, V. & Rasio, F. A. (2011), 'Twin binaries: Studies of stability, mass transfer, and coalescence', *The Astrophysical Journal* **737**(2), 49.

MacLeod, M., Ostriker, E. C. & Stone, J. M. (2018), 'Runaway coalescence at the onset of common envelope episodes', *arXiv preprint arXiv:1803.03261* .

Meyer, F. & Meyer-Hofmeister, E. (1979), 'Formation of cataclysmic binaries through common envelope evolution', *Astronomy and Astrophysics* **78**, 167–176.

Nandez, J. L., Ivanova, N. & Lombardi Jr, J. C. (2014), 'V1309 Sco—Understanding a merger', *The Astrophysical Journal* **786**(1), 39.

Nariai, K. & Sugimoto, D. (1976), 'Unstable mass outflow from a binary system', *Publications of the Astronomical Society of Japan* **28**, 593–598.

Paczynski, B. (1976), Common envelope binaries, *in* 'Symposium-International Astronomical Union', Vol. 73, Cambridge University Press, pp. 75–80.

Pejcha, O. (2014), 'Burying a binary: Dynamical mass loss and a continuous optically thick outflow explain the candidate stellar merger V1309 Scorpii', *The Astrophysical Journal* **788**(1), 22.

Pejcha, O., Metzger, B. D. & Tomida, K. (2016*a*), 'Binary stellar mergers with marginally bound ejecta: excretion discs, inflated envelopes, outflows, and their luminous transients', *Monthly Notices of the Royal Astronomical Society* **461**(3), 2527–2539.

Pejcha, O., Metzger, B. D. & Tomida, K. (2016*b*), 'Cool and luminous transients from mass-losing binary stars', *Monthly Notices of the Royal Astronomical Society* **455**(4), 4351–4372.

Pejcha, O., Metzger, B. D., Tyles, J. G. & Tomida, K. (2017), 'Pre-explosion spiral mass loss of a binary star merger', *The Astrophysical Journal* **850**(1), 59.

Sana, H., de Mink, S., de Koter, A., Langer, N., Evans, C., Gieles, M., Gosset, E., Izzard, R., Le Bouquin, J.-B. & Schneider, F. (2012), 'Binary interaction dominates the evolution of massive stars', *Science* **337**(6093), 444–446.

Sepinsky, J., Willems, B., Kalogera, V. & Rasio, F. (2009), 'Interacting binaries with eccentric orbits. II. Secular orbital evolution due to non-conservative mass transfer', *The Astrophysical Journal* **702**(2), 1387.

Shu, F. H., Anderson, L. & Lubow, S. H. (1979), 'On the structure of contact binaries. III-Mass and energy flow', *The Astrophysical Journal* **229**, 223–241.

Smith, N. (2014), 'Mass loss: its effect on the evolution and fate of high-mass stars', *Annual Review of Astronomy and Astrophysics* **52**, 487–528.

Tauris, T. & Van Den Heuvel, E. (2006), 'Formation and evolution of compact stellar X-ray sources', *Compact stellar X-ray sources* **39**, 623–665.

Tylenda, R., Hajduk, M., Kamiński, T., Udalski, A., Soszyński, I., Szymański, M., Kubiak, M., Pietrzyński, G., Poleski, R., Ulaczyk, K. et al. (2011), 'V1309 Scorpii: merger of a contact binary', *Astronomy & Astrophysics* **528**, A114.

Tylenda, R. & Kamiński, T. (2016), 'Evolution of the stellar-merger red nova V1309 Scorpii: Spectral energy distribution analysis', *Astronomy & Astrophysics* **592**, A134.

Van Rensbergen, W., De Greve, J., De Loore, C. & Mennekens, N. (2008), 'Spin-up and hot spots can drive mass out of a binary', *Astronomy & Astrophysics* **487**(3), 1129–1138.

Van Rensbergen, W., De Greve, J., Mennekens, N., Jansen, K. & De Loore, C. (2010), 'Mass loss out of close binaries - Case A Roche lobe overflow', *Astronomy & Astrophysics* **510**, A13.

Webbink, R. (1976), 'The evolution of low-mass close binary systems. I-The evolutionary fate of contact binaries', *The Astrophysical Journal* **209**, 829–845.

Zhu, L.-Y., Zhao, E.-G. & Zhou, X. (2016), 'A low-mass-ratio and deep contact binary as the progenitor of the merger V1309 Sco', *Research in Astronomy and Astrophysics* **16**(4), 068.

LIST OF FIGURES

LIST OF ABBREVIATIONS

RLOF	Roche lobe overflow
L1 point	inner/first Lagrange point
L2 point	outer/second Lagrange point
L3 point	third Lagrange point
L4 point	fourth Lagrange point
L5 point	fifth Lagrange point